The effect of solute concentration on hindered gradient diffusion in polymeric gels

By KRISTAN K. S. BUCK[1], STEPHANIE R. DUNGAN[1,2]
AND RONALD J. PHILLIPS[1]†

[1] Department of Chemical Engineering and Materials Science,
[2] Department of Food Science and Technology, University of California,
Davis, CA 95616, USA

The effect of solute concentration on hindered diffusion of sphere-like colloidal solutes in stiff polymer hydrogels is examined theoretically and experimentally. In the theoretical development, it is shown that the presence of the gel fibres enhances the effect of concentration on the thermodynamic driving force for gradient diffusion, while simultaneously reducing the effect of concentration on the hydrodynamic drag. The result is that gradient diffusion depends more strongly on solute concentration in gels than it does in pure solution, by an amount that depends on the partition coefficient and hydraulic permeability of the gel–solute system. Quantitative calculations are made to determine the concentration-dependent diffusivity correct to first order in solute concentration. In order to compare the theoretical predictions with experimental data, rates of diffusion have been measured for nonionic micelles and globular proteins in solution and agarose hydrogels at two gel concentrations. The measurements were performed by using holographic interferometry, through which one monitors changes in refractive index as gradient diffusion takes place within a transparent gel. If the solutes are modelled as spheres with short-range repulsive interactions, then the experimentally measured concentration dependence of the diffusivities of both the protein and micelles is in good agreement with the theoretical predictions.

1. Introduction

Hindered diffusion refers to the diffusion of compact macromolecules through pores or interfibre spaces of comparable size (Deen 1987). Like Brownian diffusion in a pure liquid, this transport process is driven by a gradient in chemical potential that is caused by a gradient in the solute concentration, and is resisted by the hydrodynamic drag on the solute. At very dilute solute concentrations, the dominant effects of the presence of a fibrous gel (or other porous medium) are to increase the hydrodynamic drag on the solute and to contribute a steric hindrance or tortuosity to its path, as described previously (Clague & Phillips 1996; Johnson *et al.* 1996). In this paper, we consider the effect of finite but low solute concentration on hindered diffusion in polymer gels, and show that solute–solute interactions are altered in such an environment through both thermodynamic and hydrodynamic mechanisms.

The effects of concentration on Brownian diffusion in pure liquids have been

† To whom correspondence should be addressed.

studied previously in some detail. In particular, Batchelor (1976, 1983) has examined diffusion in dilute colloidal systems by making an analogy between sedimentation and gradient diffusion. As shown in his earlier work (Batchelor 1972), a dilute suspension of particles sedimenting under the influence of gravity falls with a velocity that is a factor of $1 - 6.55\phi$ lower than that of a single particle, because of the particle–particle hydrodynamic interactions. Here ϕ is the volume fraction of the particles. In contrast, the chemical potential driving force for gradient diffusion increases by a factor of $1 + 8\phi$ in dilute, hard-sphere suspensions, with the net result that gradient diffusion is enhanced by a factor of $1 + 1.45\phi$ at finite but small concentrations, or where $\phi \ll 1$. The reference frame for diffusion here is such that the mean flux of volume of particles and fluid is zero.

The factors affecting hindered diffusion in gels are not nearly as well understood as those in solution, because of the complicated effects of the gel–fibre interactions. However, for rigid, porous and uncharged gels such as agarose, it seems likely that the same physical processes that combine to determine rates of diffusion in pure liquids would still be present, but in modified form. In a fibrous medium, one might anticipate that steric exclusion interactions would effectively reduce the volume available to spherical solutes, thereby enhancing the thermodynamic driving force for diffusion. In addition, the gel fibres, which are held fixed by interfibre junctions, could contribute a hydrodynamic screening which would reduce the hydrodynamic resistance contributed by solute–solute interactions. Both of these factors would tend to enhance the effect of solute concentration on hindered diffusion in gels. Thus, if this description is correct, then when normalized by its value at infinitely dilute solute concentrations one would expect the gradient diffusion coefficient in a gel to be increased by more than the solution value of $1 + 1.45\phi$. In the Sections that follow we calculate these effects quantitatively in the limit where $\phi \ll 1$, and subsequently evaluate the validity of the proposed qualitative description of diffusion in gels by comparing our predictions with new experimental measurements.

In previous work on diffusion at infinitely dilute solute concentrations (Phillips, Deen & Brady 1989, 1990; Clague & Phillips 1996; Johnson *et al.* 1996), it has been shown that the effect of the gel fibres on the hydrodynamic drag on the solute is well-described by Brinkman's equation,

$$\eta \nabla^2 \boldsymbol{u} - \nabla p = \frac{\eta}{k} \boldsymbol{u}, \tag{1}$$

where η is the solvent viscosity. Although originally proposed by Brinkman (1947) based on heuristic arguments, (1) has also been derived by renormalizing Stokes' equations in dilute porous media and neglecting any effects contributed by the detailed structure of the medium, save those that are contained in the hydraulic permeability k (Hinch 1977; Kim & Russel 1985*a*). Direct simulations have verified that (1) accurately describes screening in such dilute systems (Durlofsky & Brady 1987). In addition, under many conditions of interest, calculations of the drag on a sphere via Brinkman's equation are in good agreement with direct calculations for a sphere in a three-dimensional, disordered array of cylindrical fibres (Clague & Phillips 1996). With regard to comparisons with experimental data, it has been shown that the hydrodynamic effects captured by (1), combined with the steric or geometric effects associated with a random walk through a network of fibres, can be used to derive quantitative estimates of hindered diffusion coefficients in agarose gels (Clague & Phillips 1996; Johnson *et al.* 1996). Because of its theoretical and experimental success in describing hydrodynamic effects in fibrous gels, in this work

we use Brinkman's equation to account for the screening of sphere–sphere interactions that is induced by the presence of the gel fibres.

In order to test our quantitative predictions of the effect of concentration on hindered gradient diffusion, we have measured gradient diffusion coefficients for two spherical solutes over a range of solute and gel-fibre concentrations. Our measurements were made under conditions where non-hydrodynamic interactions between solutes are expected to be weak and of short range. The agarose that was used as a fibrous medium is a relatively stiff, nonionic polysaccharide gel that has been used previously in experiments at conditions of infinite dilution (Johnson *et al.* 1996; Kong *et al.* 1997). The measurements were performed by using holographic laser interferometry. In this method one first makes a holographic image of a gel in which there is a concentration gradient. After several hours, concentration changes in the gel cause changes in the refractive index profile, and superposition of the holographic image and the actual gel results in a pattern of interference fringes that can be analysed to yield the diffusion coefficient. The method is completely non-invasive, and has been verified previously for both liquid and gel systems (Gustafsson *et al.* 1993; Kosar & Phillips 1995; Kong *et al.* 1997).

In §2 below we first calculate to order ϕ the effect of the gel on the thermodynamic force that drives diffusion. We then calculate, again to order ϕ, the rate of sedimentation of a suspension of spherical particles in a Brinkman medium. As a part of that calculation, one must compute the solution to the problem of two sedimenting, interacting spheres. We describe Faxén laws for calculating that interaction for distant spheres, as well as our numerical method for solving the two-sphere problem at arbitrary separations, in §3. Also presented in §3 is the renormalization procedure used to ensure that the mean flow and divergence of the mean deviatoric stress are zero in the statistically homogeneous, sedimenting suspension. Our experimental technique is presented in §4, and our results are discussed and compared with theoretical predictions in §5. Section 6 consists of some concluding remarks.

2. Problem formulation

We consider a system composed of N spherical solutes and N_0 solvent molecules in a volume V of a statistically homogeneous fibrous medium. Each solute particle has volume v, each solvent molecule has volume v_0, and the fibre volume fraction ϕ_f is small, $\phi_f \ll 1$. Following the reasoning of Batchelor (1976), there is a 'thermodynamic' force $\boldsymbol{F}$ acting on the solutes given by

$$\boldsymbol{F} = -\nabla \mu_g = -\left(\frac{\partial \mu_g}{\partial n}\right)_{P,T} \nabla n, \tag{2}$$

where μ_g is the chemical potential of a solute molecule in the gel or fibrous medium, P and T are the thermodynamic pressure and temperature, and n is the number density of solutes, $n = N/V$. The thermodynamic force $\boldsymbol{F}_0$ on each solvent molecule is given by

$$\boldsymbol{F}_0 = -\nabla \mu_0 = -\left(\frac{\partial \mu_0}{\partial n}\right)_{P,T} \nabla n = -\frac{n}{n_0}\boldsymbol{F}, \tag{3}$$

where the last equality is inferred from the Gibbs–Duhem equation,

$$n_0 \frac{\partial \mu_0}{\partial n} + n\frac{\partial \mu_g}{\partial n} = 0. \tag{4}$$

In (3) and (4), μ_0 is the chemical potential of the solvent and n_0 is the number density of the solvent molecules. In this analysis the rigid, interconnected gel fibres are treated as a single particle of a species with a number density that is asymptotically close to zero. Hence, they play no role thermodynamically except to reduce the volume available to the solute and solvent molecules.

Since a uniform body force $-\boldsymbol{F}_0/v_0$ applied throughout the system produces no relative motion, one can consider a system where the solute is acted upon by an enhanced force $\boldsymbol{F}^*$, where

$$\boldsymbol{F}^* = \boldsymbol{F} \left(1 + \frac{nv}{n_0 v_0} \right) = -\frac{1 - \phi_f}{1 - \phi_g - \phi_f} \left(\frac{\partial \mu_g}{\partial \phi_g} \right)_{P,T} \nabla \phi_g \tag{5}$$

and the solvent molecules are force-free. In addition, at low Reynolds number the flux of particles is linear in the driving force, and hence the flux due to the force $\boldsymbol{F}^*$ can be found by using the 'sedimentation' coefficient $K(\phi_g; \phi_f, \beta)$. Here we define K as the sedimentation velocity of a particle in a homogeneous suspension with particle volume fraction ϕ_g through a homogeneous fibrous medium with fibre volume fraction ϕ_f, normalized by the velocity of a single particle through a Newtonian fluid with the same viscosity as that of the solvent filling the gel. The parameter β is the ratio of the solute radius to the fibre radius.

The particle flux $\boldsymbol{N}$ is therefore given by

$$\boldsymbol{N} = -\frac{K}{6\pi\eta a} \frac{\phi_g(1 - \phi_f)}{1 - \phi_g - \phi_f} \left(\frac{\partial \mu_g}{\partial \phi_g} \right)_{P,T} \nabla n, \tag{6}$$

whence the scalar diffusivity D is identified as

$$D = \frac{K}{6\pi\eta a} \frac{\phi_g(1 - \phi_f)}{1 - \phi_g - \phi_f} \left(\frac{\partial \mu_g}{\partial \phi_g} \right)_{P,T}. \tag{7}$$

The flux in (6) is relative to zero-volume-flux axes, which is the same as being relative to the rigidly interconnected fibres. In this development it has been assumed that the solutes are spheres and the fibrous medium is isotropic, so that the diffusivity tensor can be represented as $D\boldsymbol{I}$, where $\boldsymbol{I}$ is the identity tensor. In addition, it has been tacitly assumed that the concentration gradient is small enough so that $L|\nabla \log n| \ll 1$ and is constant over a region of gel with dimension L, so that each particle in the volume V experiences the same thermodynamic driving force. In the limit where $\phi_f \to 0$, the sedimentation coefficient K becomes $1 - 6.55\phi_g + O(\phi_g^2)$ and $\phi_g(\partial \mu_g/\partial \phi_g)_{P,T} = kT(1 + 7\phi_g + O(\phi_g^2))$, and hence (7) becomes the well-known result derived by Batchelor (1976),

$$D = \frac{kT}{6\pi\eta a} \left(1 + 1.45\phi_g + O(\phi_g^2) \right) \quad \text{as} \quad \phi_f \to 0. \tag{8}$$

In the limit $\phi_g \to 0$ but ϕ_f finite, (7) accurately predicts the infinite-dilution hindered diffusion coefficient D_0 in gels if the right-hand side is multiplied by a steric hindrance or tortuosity factor (Clague & Phillips 1996; Johnson *et al.* 1996). When the effect of concentration on the chemical potential is accounted for explicitly, as in (7), this steric factor is independent of solute concentration, and hence does not affect the concentration dependence of D/D_0 that is of interest here.

From (7) and the development leading to (8), it is clear that the dependence on concentration of the rate of hindered diffusion in a gel requires quantitative expressions for the modified sedimentation coefficient K and the derivative $(\partial \mu_g/\partial \phi_g)_{P,T}$

of the chemical potential in the gel. Evaluation of the latter term is facilitated by considering a bulk phase of pure solution which is in equilibrium with the gel. As a condition of equilibrium, it must be true that the chemical potential $\mu_g(\phi_g; \phi_f, \beta)$ of the solute in the gel and $\mu_b(\phi_b)$ of that in the bulk solution are equal. Furthermore, we define a partition coefficient κ as the equilibrium ratio of the volume fraction of solute in the gel to that in the bulk solution,

$$\kappa(\phi_g; \phi_f, \beta) = \frac{\phi_g}{\phi_b} = \kappa_0 + \kappa_1 \phi_b + \cdots, \tag{9}$$

where κ_0 and κ_1 are virial coefficients. Equation (9) and the requirement that the chemical potentials be equal lead to the relation

$$\left(\frac{\partial \mu_b}{\partial \phi_b}\right)_{P,T} = (\kappa_0 + 2\kappa_1 \phi_b + \cdots) \left(\frac{\partial \mu_g}{\partial \phi_g}\right)_{P,T}. \tag{10}$$

Substituting for the derivative of the bulk chemical potential $(kT/\phi_b)(1 + 7\phi_b)$ as used in the derivation of (8), and again making use of (9), one finds that

$$\phi_g \left(\frac{\partial \mu_g}{\partial \phi_g}\right)_{P,T} = kT \left[1 + \left(7 - \frac{\kappa_1}{\kappa_0}\right) \frac{\phi_g}{\kappa_0} + O(\phi_g^2)\right]. \tag{11}$$

Partitioning of spherical solutes in fibrous matrices has been studied by Fanti & Glandt (1990). Using a superposition approximation, they show that the partition coefficient at low to moderate fibre densities can be written in terms of g_{ms}^0, the fiber–solute pair correlation function around a single fibre, according to

$$\kappa = \exp\left[l \int_0^\infty 2\pi t (g_{ms}^0(t) - 1) \, \mathrm{d}t\right]. \tag{12}$$

In (12), l is the length of fibre per unit volume of matrix. Dividing the domain of the integration into two regions, one where $0 < t < a + a_f$ (i.e. where $g_{ms}^0 = 0$) and the other where $t > a + a_f$, and writing the virial expansion $g_{ms}^0 = 1 + \phi_b g_{ms}^1(t) + \cdots$ in the region $t > a + a_f$, one finds that

$$\kappa = \kappa_0 \left[1 + \phi_b l \int_{a+a_f}^\infty 2\pi t g_{ms}^1(t) \, \mathrm{d}t + \cdots\right] \tag{13}$$

where

$$\kappa_0 = \mathrm{e}^{-(1+\beta)^2 \phi_f}. \tag{14}$$

Here β is the ratio of the sphere radius to the fibre radius, $\beta = a/a_f$. The result for the infinite-dilution partition coefficient κ_0 in (14) was first derived by Ogston (1958). From (13), one sees that $\kappa_1/\kappa_0 \sim O(\phi_f)$, and since $\phi_f \sim \phi_g$ in the current problem, the right-hand side of (11) simplifies to $kT \left(1 + (7/\kappa_0)\phi_g + O(\phi_g^2)\right)$. The evaluation of the contribution of the chemical potential term in (7) is therefore complete, and the problem becomes one of determining the sedimentation coefficient K correct to order ϕ_g. In the derivation that follows, attention is focused exclusively on the gel phase, and the subscript g is therefore dropped, it being understood that ϕ refers only to the volume fraction of solute in the gel.

3. Sedimentation in a Brinkman medium

At low solute volume fractions, the sedimentation coefficient may be expanded as

$$K(\phi) = K_0 + K_1\phi + O(\phi^2), \tag{15}$$

where K_0 is determined from the solution for a single sphere sedimenting in a Brinkman medium, and K_1 can only be obtained by accounting for two-sphere interactions. A single sphere at x_0 with radius a sedimenting with velocity U through a Brinkman medium causes velocity and pressure disturbances $u(x)$ and $p(x)$ given by (Howells 1974; Kim & Russel 1985*b*)

and

$$\left.\begin{array}{l} u(x) = \tfrac{3}{4}a[B_0(\alpha a) + a^2 B_2(\alpha a)\nabla^2]J(x - x_0) \cdot U \\[2mm] p = \tfrac{3}{2}a\eta B_0(\alpha a)U \cdot \nabla(1/r), \end{array}\right\} \tag{16}$$

where $r = |x - x_0|$, $\alpha = 1/\sqrt{k}$, $B_0(z) = 1 + z + \tfrac{1}{3}z^2$ and $B_2(z) = (\mathrm{e}^z - B_0(z))/z^2$. The term $J(x)$ in (16) is the fundamental solution to Brinkman's equation (1), given by (Howells 1974)

$$J(x) = \frac{6}{\alpha^2 r^5}\left[1 - (1 + \alpha r + \tfrac{1}{3}\alpha^2 r^2)\mathrm{e}^{-\alpha r}\right]xx + \frac{2}{\alpha^2 r^3}\left[(1 + \alpha r + \alpha^2 r^2)\mathrm{e}^{-\alpha r} - 1\right]I. \tag{17}$$

The solution for u and p in (16) is found by solving (1) subject to no-slip boundary conditions on the sphere surface, and the conditions that the velocity and pressure decay to zero far from the sphere.

To find the sedimentation coefficient K_0 from the solution (16), one makes use of the balance between the hydrodynamic drag and gravitational forces on the sphere. The drag force F_s is obtained by evaluating the integral

$$F_s = -\int_{S_p} \Pi \cdot n \, \mathrm{d}S, \tag{18}$$

where S_p is the sphere surface and $\Pi = -pI + \eta(\nabla u + \nabla u^t)$. The result is (Solomentsev & Anderson 1996)

$$F_s = 6\pi\eta a\left(1 + \alpha a + \tfrac{1}{9}\alpha^2 a^2\right)U, \tag{19}$$

from which one finds that

$$K_0 = \frac{1}{1 + \alpha a + \tfrac{1}{9}\alpha^2 a^2}. \tag{20}$$

Interestingly, for the force on a sphere fixed in place in a uniform imposed flow, the $\tfrac{1}{9}\alpha^2 a^2$ term in (19) becomes $\tfrac{1}{3}\alpha^2 a^2$. As discussed by Solomentsev & Anderson (1996), the reason for the difference is that a constant, imposed flow in a Brinkman medium requires a corresponding imposed pressure gradient, and the latter exerts a force on the sphere that is not present when the medium is quiescent and the sphere is moving.

3.1. *Faxén laws in a Brinkman medium*

In order to calculate the term K_1 in (15), it is necessary to have Faxén laws that yield the force on a spherical particle caused by the disturbance flow produced by a second, distant particle. Such laws have been derived previously by Howells (1974) and Kim & Russel (1985*b*) for fixed particles in an imposed flow. However, without some modification, those expressions are not appropriate for our purposes. At the end of this Section we compare those expressions with the ones derived here.

Following Brenner (1964), we make use of the reciprocal theorem to derive a Faxén

law for the force on a sphere in a Brinkman medium. Consider two velocity fields $\boldsymbol{u}$ and $\boldsymbol{v}$ which, with their associated pressure fields p and q, are solutions to (1). The velocity $\boldsymbol{u}$ is that around a sphere moving with velocity $\boldsymbol{U}$ as given in (16), while $\boldsymbol{v}$ is an imposed, disturbance velocity field. From mass conservation we have that

$$\nabla \cdot \boldsymbol{u} = 0 \quad \text{and} \quad \nabla \cdot \boldsymbol{v} = 0, \tag{21}$$

and the stresses associated with the two velocities are given by $\boldsymbol{\Pi}$ and $\boldsymbol{\sigma}$, where

$$\boldsymbol{\Pi} = -p\boldsymbol{I} + \eta(\nabla\boldsymbol{u} + \nabla\boldsymbol{u}^t) \tag{22}$$

and

$$\boldsymbol{\sigma} = -q\boldsymbol{I} + \eta(\nabla\boldsymbol{v} + \nabla\boldsymbol{v}^t). \tag{23}$$

By following the usual procedure for deriving the reciprocal theorem (Deen 1998), and making use of the fact that $\nabla \cdot \boldsymbol{\sigma} = \eta\alpha^2\boldsymbol{v}$ and $\nabla \cdot \boldsymbol{\Pi} = \eta\alpha^2\boldsymbol{u}$, one finds that

$$\int_{S_p} \boldsymbol{u}(\boldsymbol{n} \cdot \boldsymbol{\sigma}) \, \mathrm{d}S = \int_{S_p} \boldsymbol{v}(\boldsymbol{n} \cdot \boldsymbol{\Pi}) \, \mathrm{d}S, \tag{24}$$

which has the same form as the reciprocal theorem normally used for Stokes equations. In deriving (24) it has been assumed that the velocities and stresses decay to zero far from the particle, so that any integrals over surfaces infinitely far from the particle are negligible.

By making use of (16) and (22), one finds that

$$\boldsymbol{n} \cdot \boldsymbol{\Pi} = \boldsymbol{U} \cdot \left\{ \boldsymbol{I}\tfrac{3}{2}(1 + \alpha a) + \tfrac{1}{2}\alpha^2 a^2 \boldsymbol{xx} \right\} \quad \text{at } r = a \tag{25}$$

for a single sphere moving with velocity $\boldsymbol{U}$. Since $\boldsymbol{u} = \boldsymbol{U}$ on S_p and since the sphere velocity $\boldsymbol{U}$ is arbitrary, substitution of (25) into (24) yields for the force $\boldsymbol{F}_v$ induced by the velocity disturbance $\boldsymbol{v}$

$$\boldsymbol{F}_v = \int_{S_p} \boldsymbol{v} \cdot \left\{ \boldsymbol{I}\tfrac{3}{2}(1 + \alpha a) + \tfrac{1}{2}\alpha^2 a^2 \boldsymbol{xx} \right\} \mathrm{d}s. \tag{26}$$

If $\boldsymbol{v}$ varies smoothly around S_p, then it can be expanded in a Taylor series about the sphere centre $\boldsymbol{x}_0$, yielding

$$\boldsymbol{v} = \boldsymbol{v}|_{\boldsymbol{x}_0} + \boldsymbol{x} \cdot \nabla\boldsymbol{v}|_{\boldsymbol{x}_0} + \tfrac{1}{2}\boldsymbol{xx} : \nabla\nabla\boldsymbol{v}|_{\boldsymbol{x}_0} + \cdots. \tag{27}$$

Substituting this result into (26) and evaluating the integrals yields

$$\boldsymbol{F}_v = 6\pi\eta a\left\{ [1 + \alpha a + \tfrac{1}{9}\alpha^2 a^2]\boldsymbol{v}|_{\boldsymbol{x}_0} + \tfrac{1}{6}[1 + \alpha a + \tfrac{7}{60}\alpha^2 a^2 + O(\alpha^3 a^3)]\nabla^2\boldsymbol{v}|_{\boldsymbol{x}_0} \right\}, \tag{28}$$

which is the desired Faxén law for the force.

An entirely analogous procedure can be followed to find a Faxén law for the torque caused by $\boldsymbol{v}$. However, instead of $\boldsymbol{u}$ corresponding to the flow around a translating sphere, we let it equal the flow around a sphere rotating with angular velocity $\boldsymbol{\Omega}$ in a quiescent Brinkman medium, given by $p = 0$ and (Solomentsev & Anderson 1996)

$$\boldsymbol{u} = \boldsymbol{\Omega} \times \boldsymbol{x} \frac{\mathrm{e}^{\alpha(a-r)}}{r^3} \left(\frac{1 + \alpha r}{1 + \alpha a} \right). \tag{29}$$

Substituting (29) into (22) and (24) and evaluating the resulting surface integrals yields for the torque

$$\boldsymbol{L}_v = 8\pi\eta a^3 \frac{1 + \alpha a + \tfrac{1}{3}\alpha^2 a^2}{1 + \alpha a} \boldsymbol{\omega}(\boldsymbol{x}_0), \tag{30}$$

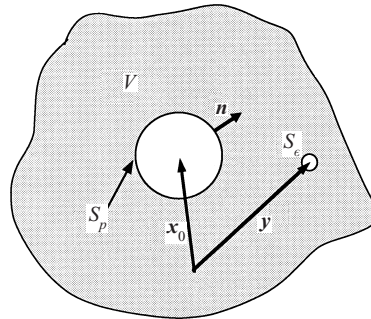where $\boldsymbol{\omega} = (\tfrac{1}{2})\nabla \times \boldsymbol{v}$ is the vorticity of the disturbance flow.

FIGURE 1. The volume V surrounding the spherical surfaces S_p and S_ε, the latter surrounding a point singularity at position y.

Equations (28) and (30) differ from the Faxén laws given previously (Howells 1974; Kim & Russel 1985b). We therefore consider a different method of derivation that yields the earlier forms, and then reconcile the two with one another. As shown in figure 1, we now consider a volume V that is outside both a spherical particle at x_0 with surface S_p and a point singularity with strength F_s at y. The point singularity is surrounded by a surface S_ε, and the volume inside the spherical particle is denoted by V_p. We again let the velocity u and stress Π correspond to the disturbance around a sphere translating with velocity U. However, here v and σ are the velocity and stress caused by the singularity at y plus a collection of image singularities in V_p which are chosen to yield $v = 0$ on S_p.

Applying the reciprocal theorem (24) to the system shown in figure 1, and using the boundary condition that $u = U$ and $v = 0$ on S_p, one finds that

$$U \cdot F_v + \int_{S_\varepsilon} u \cdot (\sigma \cdot n) \, \mathrm{d}S = \int_{S_\varepsilon} v \cdot (\Pi \cdot n) \, \mathrm{d}S. \tag{31}$$

Shrinking the surface S_ε to a point at y, and using the fact that the velocity U is arbitrary, one finds

$$F_v = 6\pi\eta a\left\{[1 + \alpha a + \tfrac{1}{3}\alpha^2 a^2] + [\mathrm{e}^{\alpha a} - 1 - \alpha a - \tfrac{1}{3}\alpha^2 a^2]\alpha^{-2}\nabla^2\right\}$$

$$\times \left(\frac{1}{8\pi\eta}\right) J(x - y)|_{x = x_0} \cdot F_s. \tag{32}$$

The $J \cdot F_s$ term in (32) is just the velocity disturbance caused by the singularity at y evaluated at the sphere centre x_0. Since any velocity disturbance v can be created by superposing a collection of singularities, that term can be replaced by the more general disturbance $v|_{x = x_0}$, yielding a result with the same form as (28), but differing in the terms that are $O(\alpha^2 a^2)$. Equation (32) is the Faxén law given by Howells (1974) and Kim & Russel (1985b).

The two forms (28) and (32) can be reconciled if one considers that, in the latter derivation, image singularities inside the volume V_p are required to move the fluid in V_p such that $v = 0$ on S_p. The region V_p inside S_p must therefore contain a Brinkman medium, and this flow results in a force density $\eta\alpha^2 v$ everywhere inside the sphere, which provides a correction to (32). Evaluation of the required volume integral is complicated by the presence of the singularities, whose positions and strengths are in

general unknown. However, that problem can be circumvented by noting that

$$\int_{V_p} \eta \alpha^2 \boldsymbol{v} \, \mathrm{d}V = \eta \alpha^2 \int_{V_p} \boldsymbol{\nabla} \cdot (\boldsymbol{vx}) \, \mathrm{d}V = \eta \alpha^2 \int_{S_p} \boldsymbol{n} \cdot (\boldsymbol{vx}) \, \mathrm{d}S. \tag{33}$$

Having expressed the correction as a surface integral, provided that the singularity at $\boldsymbol{y}$ is not too close to the sphere, the velocity $\boldsymbol{v}$ can again be written as the Taylor expansion (27). Substituting that expansion into the surface integral in (33) and evaluating the terms yields a correction of

$$-\tfrac{4}{3}\pi\eta a^3 \alpha^2 \boldsymbol{v}|_{\boldsymbol{x}_0} - \tfrac{4}{30}\pi\eta\alpha^2 a^5 \nabla^2 \boldsymbol{v}|_{\boldsymbol{x}_0}, \tag{34}$$

which when added to the right-hand side of (32) yields (28).

To apply the singularity method to the derivation of a Faxén law for the torque, we let the velocity $\boldsymbol{u}$ correspond to that of a sphere rotating with angular velocity $\boldsymbol{\Omega}$, as given in (29). Expressed in terms of the Green's function $\boldsymbol{J}$, this velocity is

$$u_i(\boldsymbol{x}) = \left(\frac{a^3}{2}\right) \frac{\mathrm{e}^{\alpha a}}{1 + \alpha a} \Omega_m \varepsilon_{jkm} \frac{\partial}{\partial x_k} J_{ij}(\boldsymbol{x} - \boldsymbol{x}_0), \tag{35}$$

where ε_{jkm} is the permutation symbol and indicial notation has been used. In this case the reciprocal theorem (24), written over both the surfaces S_p and S_ε, reduces to

$$\boldsymbol{L}_v = 8\pi\eta a^3 \frac{\mathrm{e}^{\alpha a}}{1 + \alpha a} \boldsymbol{\omega}(\boldsymbol{x}_0) \tag{36}$$

where again $\boldsymbol{\omega} = \tfrac{1}{2}\boldsymbol{\nabla} \times \boldsymbol{v}$ is the vorticity of the velocity field $\boldsymbol{v}$.

As in the force problem, the flow in the Brinkman medium inside V_p induces a torque correction of

$$\int_{V_p} \boldsymbol{x} \times \eta \alpha^2 \boldsymbol{v} \, \mathrm{d}V, \tag{37}$$

and accounting for this term reconciles (36) and (30). In this case, the correction term cannot be simply recast into a surface integral. However, the largest portion of the flow field $\boldsymbol{v}$ inside V_p that causes a torque is the flow due to a point-torque at $\boldsymbol{x}_0$ that cancels the rotation $\boldsymbol{\omega}$ on S_p, and can be evaluated by substituting $\boldsymbol{\omega}$ for $\boldsymbol{\Omega}$ in (29). Substituting the resulting expression for $\boldsymbol{v}$ into (37) and evaluating the volume integral yields a correction of

$$-\frac{8\pi\eta a^3}{3} \left[\frac{\mathrm{e}^{\alpha a} - (1 + \alpha a)}{1 + \alpha a}\right] \boldsymbol{\omega}(\boldsymbol{x}_0) \tag{38}$$

which, when added to the right-hand side of (36), yields (30) to $O(\alpha^2 a^2)$.

The preceding discussion shows that, when an imposed flow $\boldsymbol{v}$ and its associated stress decay to zero far from a particle, the correct Faxén law for determining the resulting force is (28). Equation (32) contains a contribution from flow inside the particle which is not appropriate for a hard-sphere solute. Using (28) together with (19) shows that a velocity disturbance $\boldsymbol{v}$ causes a force-free sphere at $\boldsymbol{x}_0$ to translate with a velocity $\boldsymbol{v}(\boldsymbol{x}_0)$, plus a correction due to the Laplacian term. Similarly, a torque-free sphere rotates with angular velocity $\boldsymbol{\omega}(\boldsymbol{x}_0)$. Because the divergence of the stress is not zero in a Brinkman medium, when a disturbance flow acts on a particle, the strength of a force singularity at the sphere centre needed to cancel the disturbance velocity on the surface is greater than the actual surface force as given by (18). Equation (32), with $\boldsymbol{J} \cdot \boldsymbol{F}$ replaced by $\boldsymbol{v}$, yields the strength of such a singularity.

It also yields the actual surface force for a flow field driven by a pressure gradient imposed far from the sphere, since the contribution of the imposed pressure gradient cancels the correction (33) for the flow in V_p.

3.2. *The renormalization procedure*

Following Batchelor (1972), the average change $\overline{U}'$ in the velocity of a test sphere at x_0 caused by the presence of N spheres in the configuration C_N is given by

$$\overline{U}' = \frac{1}{N!} \int U'(x_0, C_N) P(C_N | x_0) \, dC_N. \tag{39}$$

Here $P(C_N | x_0)$ is the probability of configuration C_N given that a sphere is at x_0, and $dC_N = dr_1 \dots dr_N$ is an integration over the positions of all N spheres. The velocity change U' for a particular configuration is found from the Faxén law (28) to be

$$U'(x_0, C_N) = \frac{1}{A_0(\alpha a)}(A_0(\alpha a) + a^2 A_2(\alpha a)\nabla^2)u(x, C_N)|_{x=x_0}, \tag{40}$$

where $A_0(z) = 1 + z + \frac{1}{9}z^2$, $A_2(z) = \frac{1}{6}\left(1 + z + \frac{7}{60}z^2\right)$, and u is the fluid velocity disturbance caused by the N spheres.

Expressing $u(x, C_N)$ as the superposition of the velocity disturbances from each sphere in the dilute suspension, and using that for a dilute suspension

$$P(C_N | x_0) \approx P(x_0 + r_k | x_0) P(C_{N-1}), \tag{41}$$

where $x_0 + r_k$ is the position of the centre of the kth sphere, (39) can be simplified to

$$\overline{U}' = \int_{r \geqslant 2a} U'(x_0, x_0 + r) P(x_0 + r | x_0) \, dr. \tag{42}$$

In sedimentation through a pure fluid, the disturbance U' decays as $1/r$, and hence the integral in (42) is not convergent. Physically this difficulty may be attributed to the fact that, for widely separated spheres, it is inappropriate to calculate two-sphere interactions as if they occurred through a pure fluid. Batchelor (1972) successfully evaluated $\overline{U}'$ by renormalizing the divergent integral. The renormalization is achieved by using the physical insights that the mean flow and the divergence of the mean deviatoric stress are zero in a statistically homogeneous suspension. With this information, the integral in (42) over the unbounded space $r \geqslant 2a$ can be re-expressed in terms of integrals in the region $0 \leqslant r \leqslant 2a$, which yield a finite result.

When two spheres interact through a Brinkman medium, the disturbance U' decays more rapidly than $1/r$ as a result of Brinkman screening. For widely separated spheres, the most slowly decaying part of the velocity disturbance from a sphere at $x_0 + r$ is $(\frac{1}{8}\pi\eta)J(r) \cdot F$, where F is the gravitational force $(4\pi/3)a^3\Delta\rho g$, g being gravity and $\Delta\rho$ the density difference between the particles and the Brinkman medium. From (17), one sees therefore that U' decays as $1/r^3$ in the current problem, a rate that still leads to convergence difficulties. If the angular integrations in (42) are performed first, one finds that the $O(1/r^3)$ terms cancel and the integrand decays exponentially, making the integral convergent. Nonetheless, (42) is still missing important physical aspects of the sedimentation problem.

For two widely separated spheres in a suspension sedimenting through a Brinkman medium, the sphere–sphere interaction cannot be calculated via a two-sphere problem which does not account for the other particles. To see this, consider that far from a test sphere located at x_0, averaging the effect of a second sphere at $x_0 + r$ is equivalent

to placing a uniform distribution of point forces and quadrupoles throughout the Brinkman medium (cf. (16)). A distribution of point forces with strength $\boldsymbol{F}$ in an unbounded medium drives a net flow proportional to $n\boldsymbol{F}/\eta\alpha^2$, where n is the number density of particles. Although this flow is finite since $\alpha^2 > 0$ in a Brinkman medium, clearly in actual sedimentation in a container with a bottom there must be zero mean flow, a characteristic that is missed in straightforward application of (42). One consequence of this failure is that (42) predicts that a suspension in a Brinkman medium would have a settling velocity that is faster than that of a single particle. To avoid this problem, and a similar difficulty with the divergence of the mean deviatoric stress, we follow the renormalization procedure of Batchelor (1972). In other words, we use known, mean properties of the suspension to change the domain of integration in (42) from being infinite to finite, using the two-sphere problem only to calculate local interactions.

We begin by subtracting the far-field interaction terms from $\boldsymbol{U}'$ in (39) and placing them in a separate term, as follows:

$$\overline{\boldsymbol{U}}' = \frac{1}{N!} \int \left[\boldsymbol{U}'(\boldsymbol{x}_0, C_N) - \frac{1}{A_0}(A_0 + a^2 A_2 \nabla^2)\boldsymbol{u}(\boldsymbol{x}, C_N)|_{\boldsymbol{x}=\boldsymbol{x}_0} \right] P(C_N|\boldsymbol{x}_0)\,\mathrm{d}C_N$$

$$+ \frac{1}{N!} \int \frac{1}{A_0}(A_0 + a^2 A_2 \nabla^2)\boldsymbol{u}(\boldsymbol{x}, C_N)|_{\boldsymbol{x}=\boldsymbol{x}_0} P(C_N|\boldsymbol{x}_0)\,\mathrm{d}C_N. \quad (43)$$

We refer to the first integral in (43) as $\boldsymbol{W}$. It contains only short-range interactions, and is calculated numerically in the next Section. The second integral, which we denote by $\boldsymbol{V}$, is to be re-expressed as an integral over a finite domain as discussed above.

The velocity $\bar{\boldsymbol{u}}(\boldsymbol{x})$ averaged over the fluid and particles can be written as

$$\bar{\boldsymbol{u}}(\boldsymbol{x}) = \frac{1}{N!} \int \boldsymbol{u}(\boldsymbol{x}, C_N) P(C_N)\,\mathrm{d}C_N = 0, \quad (44)$$

where the last equality expresses the fact that the mean velocity is zero. Similarly, as noted by Batchelor (1972), the mean value of the deviatoric stress $\boldsymbol{\tau} = \boldsymbol{\Pi} - (\frac{1}{3})p\boldsymbol{I}$ is constant in a statistically homogeneous, sedimenting suspension, and hence its divergence must be zero, so that

$$\frac{1}{N!} \int \nabla \cdot \boldsymbol{\tau}(\boldsymbol{x}, C_N) P(C_N)\,\mathrm{d}C_N = 0. \quad (45)$$

Note that $\nabla \cdot \boldsymbol{\tau}$ is equal to $\eta \nabla^2 \boldsymbol{u}$ in the fluid phase.

Since the integrals in (44) and (45) are zero, they can be subtracted from the second integral in (43), yielding

$$\boldsymbol{V}(\boldsymbol{x}_0, C_N) = \frac{1}{N!} \int \boldsymbol{u}(\boldsymbol{x}_0, C_N)[P(C_N|\boldsymbol{x}_0) - P(C_N)]\,\mathrm{d}C_N$$

$$+ \frac{1}{N!} \int \frac{a^2 A_2}{A_0} \{\nabla^2 \boldsymbol{u}(\boldsymbol{x}, C_N)\}_{\boldsymbol{x}=\boldsymbol{x}_0} P(C_N|\boldsymbol{x}_0)\,\mathrm{d}C_N$$

$$- \frac{a^2 A_2}{\eta A_0} \frac{1}{N!} \left\{ \int \nabla \cdot \boldsymbol{\tau}(\boldsymbol{x}, C_N) P(C_N)\,\mathrm{d}C_N \right\}_{\boldsymbol{x}=\boldsymbol{x}_0}. \quad (46)$$

The integral over $\nabla \cdot \boldsymbol{\tau}$ in (46) can be simplified by first noting that

$$P(C_N) = P(C_{N-1}|\boldsymbol{x}_0 + \boldsymbol{r}_k)P(\boldsymbol{x}_0 + \boldsymbol{r}_k) = P(C_{N-1}|\boldsymbol{x}_0 + \boldsymbol{r}_k)n \quad (47)$$

and $dC_N = dr_k dC_{N-1}$. The integral over dr_k can then be separated into two regions, one where $|x_0 + r_k - x| \leqslant a$ (i.e. x is inside the kth sphere) and one where $|x_0 + r_k - x| \geqslant a$ (i.e. x is outside the kth sphere). This yields

$$\frac{1}{N!} \int \nabla \cdot \boldsymbol{\tau}(x, C_N) P(C_N) \, dC_N$$

$$= \frac{1}{N!} \int \int_{|x_0 + r_k - x| \leqslant a} \nabla \cdot \boldsymbol{\tau}(x, C_N) P(C_{N-1} | x_0 + r_k) n \, dr_k \, dC_{N-1}$$

$$+ \frac{1}{N!} \int \int_{|x_0 + r_k - x| \geqslant a} \nabla \cdot \boldsymbol{\tau}(x, C_N) P(C_{N-1} | x_0 + r_k) n \, dr_k \, dC_{N-1}. \quad (48)$$

Proceeding to separate out the integrals over the interiors of all the N spheres, as is done with the kth sphere in (48), converts the first integral on the right-hand side of (48) to a sum from 1 to N. In addition, the second integral is restricted to points x in the fluid phase, where $|x_0 + r_k - x| \geqslant a$ for all values of k, so that $\nabla \cdot \boldsymbol{\tau}$ may be replaced by $\eta \nabla^2 u$. The right-hand side of (48) is then

$$\sum_{k=1}^{N} \frac{n}{N!} \int \boldsymbol{f}(x_0 + r_k, C_{N-1}) P(C_{N-1} | x_0 + r_k) \, dC_{N-1}$$

$$+ \frac{1}{N!} \int_{|x_0 + r_k - x| > a, \, \text{all } k} \eta \nabla^2 u(x, C_N) P(C_N) \, dC_N, \quad (49)$$

where the integrals of $\nabla \cdot \boldsymbol{\tau}$ over the interiors of the spheres have been converted to surface integrals of the force density $\boldsymbol{n} \cdot \boldsymbol{\tau}$ by using the divergence theorem, and evaluated. The integral of $\boldsymbol{n} \cdot \boldsymbol{\tau}$ over the sphere surfaces yields, to leading order, the viscous stress on an isolated, sedimenting sphere, which is $\boldsymbol{f} = -4\pi \eta a U_0 (1 + \alpha a)$ in a Brinkman medium (Howells 1974).

Substitution of (49) into (46) yields a renormalized expression for the far-field velocity correction V:

$$V(x_0, C_N) = \frac{1}{N!} \int u(x_0, C_N) [P(C_N | x_0) - P(C_N)] \, dC_N - \frac{n a^2 A_2(\alpha a)}{\eta A_0(\alpha a)} \boldsymbol{f}$$

$$+ \frac{1}{N!} \int_{r_k > a} \frac{a^2 A_2(\alpha a)}{A_0(\alpha a)} \{\nabla^2 u(x, C_N)\}_{x = x_0} [P(C_N | x_0) - P(C_N)] \, dC_N, \quad (50)$$

where the integral over $\boldsymbol{f}$ has been evaluated by using that $P(C_{N-1} | x_0 + r_k) \approx P(C_{N-1})$ in a dilute suspension. Also, because the second integral in (50) is independent of x, there x has been set equal to x_0.

By writing $u(x_0, C_N)$ as a sum of contributions from the N spheres, and using that

$$P(C_N | x_0) - P(C_N) = P(x_0 + r_k | x_0) P(C_{N-1} | x_0, x_0 + r_k) - P(x_0 + r_k) P(C_{N-1} | x_0 + r_k)$$

$$\approx [P(x_0 + r_k | x_0) - P(x_0 + r_k)] P(C_{N-1}) \quad (51)$$

in a dilute suspension, (50) simplifies further to

$$V = \int_r u(x_0, x_0 + r) [P(x_0 + r | x_0) - P(x_0 + r)] \, dr - \frac{n a^2 A_2(\alpha a)}{\eta A_0(\alpha a)} \boldsymbol{f}$$

$$+ \int_{r > a} \frac{a^2 A_2(\alpha a)}{A_0(\alpha a)} \{\nabla^2 u(x, x + r)\}_{x = x_0} [P(x_0 + r | x_0) - P(x_0 + r)] \, dr. \quad (52)$$

Now we make use of the relations

$$P(\mathbf{x}_0 + \mathbf{r}|\mathbf{x}_0) = \begin{cases} 0 & \text{for} \quad r < 2a \\ n & \text{for} \quad r > 2a \end{cases} \tag{53}$$

and

$$P(\mathbf{x}_0 + \mathbf{r}) = n \quad \text{for all} \quad r. \tag{54}$$

In addition, we know that $\mathbf{u} = \mathbf{U}_0$ for $r < a$ and that $\mathbf{u}$ is given by (16) for $r > a$. Equation (52) can then be written as

$$\mathbf{V} = -\phi \mathbf{U}_0 - 3\phi \mathbf{U}_0 \frac{A_2(\alpha a)}{A_0(\alpha a)}(1 + \alpha a) - \frac{3na}{4} \int_{a < r < 2a} (B_0 + a^2 B_2 \nabla^2) \mathbf{J} \cdot \mathbf{U}_0 \, \mathrm{d}\mathbf{r}$$

$$-\frac{3na^3}{4} \frac{A_2(\alpha a)}{A_0(\alpha a)} \int_{a < r < 2a} \nabla^2 (B_0 + a^2 B_2 \nabla^2) \mathbf{J} \cdot \mathbf{U}_0 \, \mathrm{d}\mathbf{r}, \tag{55}$$

where $\mathbf{U}_0$ is the velocity of an isolated sphere in a Brinkman medium. The last integral in (55) can be conveniently simplified by noting that

$$(B_0 + a^2 B_2 \nabla^2) \nabla^2 \mathbf{J} = (B_0 + a^2 \alpha^2 B_2) \nabla^2 \mathbf{J} = \mathrm{e}^{\alpha a} \nabla^2 \mathbf{J}. \tag{56}$$

Evaluating the integrals in (55) yields

$$\mathbf{V} = -\phi \mathbf{U}_0 - 3\phi \mathbf{U}_0 \left(\frac{1}{\alpha^2 a^2} \right) [(1 + \alpha a) - \mathrm{e}^{-\alpha a}(1 + 2\alpha a)]$$

$$+ 3\phi \mathbf{U}_0 \left(\frac{A_2(\alpha a)}{A_0(\alpha a)} \right) \mathrm{e}^{-\alpha a}(1 + 2\alpha a). \tag{57}$$

In the limit $\alpha a \to 0$, $\mathbf{V}$ in (57) becomes equal to $-5\phi \mathbf{U}_0$, a result that is consistent with that of Batchelor (1972) for sedimentation in pure fluids.

3.3. *Numerical calculation of two-sphere interactions*

We now turn our attention to the numerical calculation of $\mathbf{W}$ in (43), where

$$\mathbf{W} = \frac{1}{N!} \int \left[\mathbf{U}'(\mathbf{x}_0, C_N) - \frac{1}{A_0}(A_0 + a^2 A_2 \nabla^2) \mathbf{u}(\mathbf{x}, C_N)|_{\mathbf{x} = \mathbf{x}_0} \right] P(C_N|\mathbf{x}_0) \, \mathrm{d}C_N. \tag{58}$$

As with the far-field interaction term $\mathbf{V}$, and as described by Batchelor (1972), in a dilute suspension $\mathbf{W}$ can be simplified to a form that involves only two-sphere interactions:

$$\mathbf{W} = n \int \left[\mathbf{U}'(\mathbf{x}_0, \mathbf{x}_0 + \mathbf{r}) - \frac{1}{A_0}(A_0 + a^2 A_2 \nabla^2) \mathbf{u}(\mathbf{x}, \mathbf{x} + \mathbf{r})|_{\mathbf{x} = \mathbf{x}_0} \right] \mathrm{d}\mathbf{r}. \tag{59}$$

In (59), $\mathbf{U}'(\mathbf{x}_0, \mathbf{x}_0 + \mathbf{r})$ is the change in velocity of a sphere at $\mathbf{x}_0$ caused by a sphere at $\mathbf{x}_0 + \mathbf{r}$, a quantity which is obtained by solving numerically the problem of two spheres sedimenting in a Brinkman medium. The far-field subtraction term is evaluated analytically below.

Like Stokes equations, Brinkman's equation is linear, and the velocity $\mathbf{U}$ of a sphere at $\mathbf{x}_0$ in the presence of a second sphere at $\mathbf{x}_0 + \mathbf{r}$ can be written in the form

$$\mathbf{U} = [\lambda_1(r)\mathbf{rr} + \lambda_2(r)(\mathbf{I} - \mathbf{rr})] \cdot \mathbf{F}, \tag{60}$$

where $\mathbf{F}$ is the gravitational force on both spheres. The scalar functions $\lambda_1(r)$ and $\lambda_2(r)$ describe the behaviour when the line-of-centres between the two bodies is in
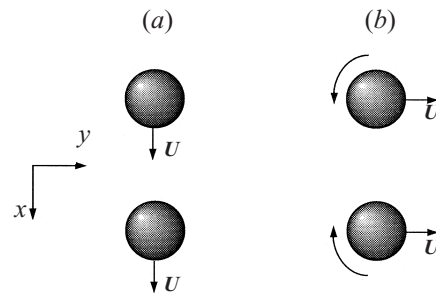
FIGURE 2. Two spheres moving (*a*) in the *x*-direction, along their line of centres, and (*b*) in the *y*-direction, perpendicular to their line of centres. The spheres moving in the *y*-direction have rotational velocities that are equal in magnitude but in opposite directions (i.e. $\pm \mathbf{e}_z$).

the direction of or perpendicular to $\mathbf{F}$, respectively. As shown in figure 2, in each configuration the two spheres have equal translational velocities in either the *x*- or *y*-direction. For the configuration in figure 2(*a*), where the spheres move in a direction parallel to their line-of-centres, their rotational velocities are zero. When the spheres move perpendicular to their line-of-centres, as shown in figure 2(*b*), they rotate in the *z*-direction with angular velocities that are equal in magnitude but in opposite directions. Determination of the two scalar functions in (60) provides the required solution to the two-sphere interaction problem in a Brinkman medium.

To obtain this solution, we make use of a singularity method that has been used successfully in the past for calculating low-Reynolds-number flows (Dabros 1985; Nitsche & Brenner 1990; Clague & Phillips 1996, 1997) and linearized-Poisson–Boltzmann electrostatic interactions (Phillips 1995). In this method, the velocity field $\mathbf{u}(\mathbf{x})$ is written as the superposition of contributions from N_f point-force singularities located inside the spheres. The strengths of the singularities are chosen so as to minimize the deviation from the no-slip boundary condition at N_s points on the sphere surfaces. For two spheres translating with velocity $\mathbf{U}$ and not rotating, this procedure yields a system of equations with the form

$$\frac{1}{8\pi\eta} \sum_{i=1}^{N_f} \mathbf{J}(\mathbf{x}_s^j - \mathbf{x}_f^i) \cdot \mathbf{f}_i = \mathbf{U}, \quad j = 1, 2 \ldots N_s, \tag{61}$$

where $\mathbf{x}_s^j$ and $\mathbf{x}_f^i$ are the positions of the *j*th surface point and *i*th singularity, respectively. The unknown quantities in (61) are the strengths $\mathbf{f}_i$ of the N_f singularities. Because two spheres sedimenting perpendicular to their line-of-centres rotate as well as translate, the determination of $\lambda_1(r)$ and $\lambda_2(r)$ also requires consideration of problems where the two spheres rotate with rotational velocities that are equal in magnitude, but in opposite directions. In that case, the right-hand side of (61) is replaced with $\pm\mathbf{\Omega} \times \mathbf{x}_s^j$.

In a singularity method of this type, the region inside the sphere surfaces is treated as a Brinkman medium which resists the fluid motion caused by the singularities. This resistance, which is a manifestation of the fact that the divergence of the stress is not zero in a Brinkman medium, results in the force on the sphere being different from the sum of the strengths of the point-force singularities. In this work, the force was calculated by direct application of (18), and the torques $\mathbf{L}$ were calculated similarly by using

$$\mathbf{L} = -\int_s \mathbf{x}_s \times (\mathbf{\Pi} \cdot \mathbf{n}) \, \mathrm{d}S, \tag{62}$$

where $\boldsymbol{x}_s$ is a vector from the sphere centre to a point on its surface. The integration was performed by using Simpson's rule with angular divisions of $\pi/80$.

To obtain the two-sphere mobility matrix, we first form the resistance matrix by imposing translational and rotational velocities on two spheres as shown in figure 2, and calculate the resulting forces and torques. We need consider only cases where the two spheres translate with equal velocities in the x-direction, translate with equal velocities in the y-direction but do not rotate, or rotate in the z-direction with rotational velocities equal in magnitude but opposite in direction. The resulting resistance matrix relates the force and torque of one of the two particles to its translational and rotational velocities according to

$$\begin{bmatrix} F_x \\ F_y \\ L_z \end{bmatrix} = \begin{bmatrix} A_{xx} & 0 & 0 \\ 0 & A_{yy} & B_{yz} \\ 0 & B_{yz} & D_{zz} \end{bmatrix} \cdot \begin{bmatrix} U_x \\ U_y \\ \Omega_z \end{bmatrix}, \qquad (63)$$

where x and y are coordinate directions as defined in figure 2. For torque-free spheres, inverting (63) yields for the mobility relation

$$\begin{bmatrix} U_x \\ U_y \end{bmatrix} = \begin{bmatrix} \dfrac{1}{A_{xx}} & 0 \\ 0 & \dfrac{-D_{zz}}{B_{yz}^2 - D_{zz}A_{yy}} \end{bmatrix} \cdot \begin{bmatrix} F_x \\ F_y \end{bmatrix}. \qquad (64)$$

In general the mobility functions $\lambda_1(r)$ and $\lambda_2(r)$ therefore correspond to $1/A_{xx}$ and $-D_{zz}/(B_{yz}^2 - D_{zz}A_{yy})$, respectively. The one exception occurs when two spheres sedimenting perpendicular to their line-of-centres are touching (i.e. $r = 2a$). In that case, the spheres do not rotate so that $\Omega_z = 0$ and $\lambda_2 = 1/A_{yy}$ (Goldman, Cox & Brenner 1966).

Based on the residual errors at the N_s surface points, this method of calculation has been found to yield accurate results to at least the fourth decimal place. Its efficacy was also verified in two other ways. First, by substituting the Green's function $\boldsymbol{G}(\boldsymbol{x})$ for Stokes flow in place of $\boldsymbol{J}(\boldsymbol{x})$ in (61), where

$$\boldsymbol{G}(\boldsymbol{x}) = \frac{\boldsymbol{I}}{r} + \frac{\boldsymbol{x}\boldsymbol{x}}{r^3}, \qquad (65)$$

the solution for two spheres interacting in a pure fluid at low Reynolds number was obtained. The resulting values for $\lambda_1(r)$ and $\lambda_2(r)$ for Stokes flow were in excellent agreement with those reported by Goldman *et al.* (1966) and Batchelor (1972). In addition, calculation of resistance functions and comparison with figures 3 and 4 of the paper by Kim & Russel (1985*b*) also showed excellent agreement between our calculation and theirs.

Our results for $\lambda_1(r)$ and $\lambda_2(r)$ for two spheres sedimenting in a Brinkman medium are plotted in figure 3(*a, b*) for several values of αa. The integral in (59) yielding $\boldsymbol{W}$ can be evaluated by using these solutions. Substituting $A_0(\alpha a)\boldsymbol{U}_0$ for $\boldsymbol{F}$ in (60), subtracting $\boldsymbol{U}_0$ in order to obtain $\boldsymbol{U}'$, and performing the angular integrations yields

$$\boldsymbol{W} = \phi \boldsymbol{U}_0 \int_2^\infty \left\{ \lambda_1 + 2\lambda_2 - 3\left[1 + \frac{1}{A_0(\alpha a)}\frac{a}{r}\right.\right.$$

$$\left.\left. \times \left(1 + \alpha a + \frac{\alpha^2 a^2}{36} + O(\alpha^3 a^3)\right) e^{\alpha(a-r)}\right]\right\} \left(\frac{r}{a}\right)^2 d\left(\frac{r}{a}\right). \qquad (66)$$

Here the term $\lambda_1 + 2\lambda_2 - 3$ contains the complete, numerically calculated two-sphere
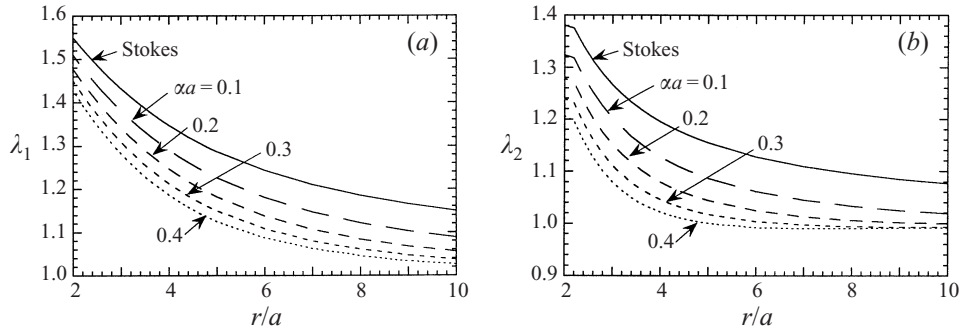
FIGURE 3. Plot of (a) $\lambda_1(r)$ and (b) $\lambda_2(r)$ for $\alpha a = 0, 0.1, 0.2, 0.3$ and 0.4.

interaction, and the remainder of the subtraction term inside the square brackets corresponds to the far-field subtraction term in the integrand of (59). As can be seen from (59), the subtraction term accounts for the point-force and quadrupole perturbations to the velocity of the test sphere at x_0 that are made by a second sedimenting sphere at $x_0 + r$.

The slowest decaying portion of the integrand in (66) is contributed by the stresslet on the sphere at $x_0 + r$ that is induced by the test sphere at x_0. The strength of this stresslet is (Kim & Russel 1985b)

$$S_{ij} = -\tfrac{20}{3}\pi\eta a^3 H(\alpha a)e'_{ij}, \tag{67}$$

where the function $H(\alpha a)$ is given by

$$H(\alpha a) = \frac{1 + \alpha a + \tfrac{2}{5}(\alpha a)^2 + \tfrac{1}{15}(\alpha a)^3}{1 + \alpha a}, \tag{68}$$

the rate-of-strain disturbance $e'_{ij} = \tfrac{1}{2}(\nabla_j u'_i + \nabla_i u'_j)$, and the disturbance velocity u' may be calculated using the point-force velocity disturbance contributed by the sphere at x_0. The velocity perturbation u^s caused by the stresslet induced on the sphere at $x_0 + r$ is given by

$$u^s_i = K_{ijk}S_{jk}, \tag{69}$$

where the propagator $K_{ijk} = \tfrac{1}{2}(\nabla_k J_{ij} + \nabla_j J_{ik})$ is directly analogous to that used in multipole moment expansions in Stokes flow calculations (Durlofsky, Brady & Bossis 1987).

Using the velocity disturbance u^s_i in conjunction with the Faxén law (28), far-field contributions to λ_1 and λ_2 beyond those included in (66) can be obtained. These contributions, which are denoted by λ^s_1 and λ^s_2, are given by

$$\lambda^s_1 = \frac{-135}{(\alpha a)^4(r/a)^8} A_0(\alpha a)H(\alpha a)\left(e^{\alpha r} - 1 - \alpha r - \tfrac{1}{3}\alpha^2 r^2\right)^2 e^{-2\alpha r} \tag{70}$$

and

$$\lambda^s_2 = \frac{-45}{(\alpha a)^4(r/a)^8} A_0(\alpha a)H(\alpha a)\left(e^{\alpha r} - 1 - \alpha r - \tfrac{1}{2}\alpha^2 r^2 - \tfrac{1}{6}\alpha^3 r^3\right)^2 e^{-2\alpha r}. \tag{71}$$

In the limit $\alpha a \to 0$, the combination $\lambda^s_1 + 2\lambda^s_2 \to -\tfrac{15}{4}(a/r)^4$, as expected from the work of Batchelor (1972). In figure 4, results from our numerical calculation of $\lambda_1 + 2\lambda_2 - 3$ are plotted along with the analytic, far-field results both with and without the stresslet
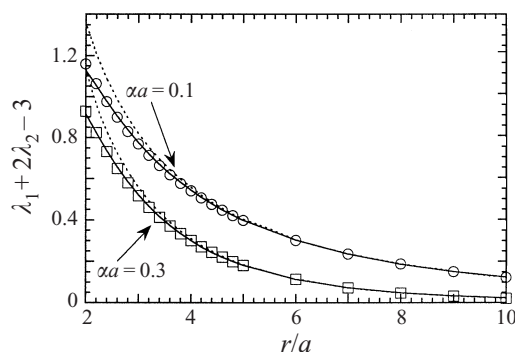
FIGURE 4. The complete numerical result for $\lambda_1 + 2\lambda_2 - 3$ ($\square$, $\bigcirc$) along with analytic, far-field approximations both with (———) and without ($\cdots\cdots$) the stresslet contribution of (70) and (71).

αa	K^v/K_0	K^w/K_0
0	-5.00	-1.55
0.1	-4.72	-1.08
0.2	-4.46	-0.52
0.3	-4.23	-0.09
0.4	-4.02	0.19

TABLE 1. Predicted effect of concentration on sedimentation in a fibrous medium.

contributions (70) and (71). The far-field result without a stresslet contribution is just the decaying portion of the subtraction term in the integrand of (66), or

$$\frac{3}{A_0(\alpha a)} \frac{a}{r} \left(1 + \alpha a + \frac{\alpha^2 a^2}{36} + O(\alpha^3 a^3) \right) e^{\alpha(a-r)}. \tag{72}$$

The agreement between the analytic and numerical results is very good even at small values of r/a. However, in spite of this good agreement, by direct calculation it has been found that accurate evaluation of the integral in (66) still requires the full numerical result over part of the domain.

To obtain results for the contribution K_1 to the sedimentation coefficient (cf. (15)), the integral in (66) was evaluated numerically for values of the radial coordinate r such that $2 \leqslant r/a \leqslant 8$, and it was evaluated analytically for $r/a > 8$ by using (70) and (71). We summarize our theoretical results by separating the coefficient K_1 of (15) into components according to $K_1 = K^v + K^w$, where K^v/K_0 is the coefficient of ϕU_0 in (57) and K^w/K_0 is the contribution of the integral in (66). These results for the sedimentation coefficient can be combined with (7) and (11) to show that the overall effect of solute concentration on the normalized diffusion coefficient D/D_0 is $\phi D_1/D_0$, where $D_1/D_0 = 1 + 7/\kappa_0 + K_1/K_0$. Here D_0 is the diffusion coefficient in the gel in the limit of infinitely dilute solute concentration. Values of K^v/K_0 and K^w/K_0 are listed for a range of permeabilities αa in table 1. We again note that the calculation for $\alpha a = 0$, which corresponds to a pure fluid, was performed with the same numerical method used for the Brinkman calculation, but with the Stokes propagator $\mathbf{G}(\mathbf{x})$ from (65) substituted for the Brinkman propagator $\mathbf{J}(\mathbf{x})$. The fact that the coefficient agrees exactly with that of Batchelor (1976) therefore confirms the accuracy of our calculations. These results can be used in combination with (12) to

determine whether the effect of concentration on gradient diffusion of hard spherical solutes is enhanced in a gel environment. Such calculations are presented in §5, where they are also compared with the experimental measurements that are described in §4.

3.4. *Incorporation of a solute–solute attraction or repulsion*

It is relatively straightforward to modify the results presented above to account for the effects of a short-range, solute–solute attraction or repulsion, as explained by Batchelor (1982) and Batchelor & Wen (1982). To that end, we introduce an interaction parameter γ defined by

$$\gamma = 3 \int_2^\infty \left\{ \exp\left(-\frac{\Phi}{kT}\right) - 1 \right\} \left(\frac{r}{a}\right)^2 \mathrm{d}\left(\frac{r}{a}\right), \tag{73}$$

where Φ is the energy of interaction between the two solutes. The interactions characterized by γ affect both the thermodynamic and hydrodynamic contributions to diffusion. The thermodynamic contribution is captured by the virial coefficient for the chemical potential, which changes from $1 + 7/\kappa_0$ for the hard-sphere case to $1 + (7 - \gamma)/\kappa_0$ in the presence of the interaction potential. Note that negative values of γ signify a solute–solute repulsion that results in an increase in the chemical potential at a given concentration.

The leading effect of concentration on the sedimentation velocity, which is given by K_1/K_0 when normalized by the velocity of a single sphere in a Brinkman medium, is altered to (Batchelor 1982; Batchelor & Wen 1982)

$$\frac{K_1}{K_0} + \int_2^\infty (\lambda_1 + 2\lambda_2 - 3) \left\{ \exp\left(-\frac{\Phi}{kT}\right) - 1 \right\} \left(\frac{r}{a}\right)^2 \mathrm{d}\left(\frac{r}{a}\right) \tag{74}$$

by the non-zero potential Φ. For interactions that are short-range such that $\exp(-\Phi/kT) - 1 \approx 0$ for $r > 2.2a$ the expression (74) can be simplified to

$$K_1/K_0 + (0.44 - 0.56\alpha a)\gamma. \tag{75}$$

This simplification is possible because the mobility terms in (74) are closely approximated by $1.32 - 1.68\alpha a$ in the region $2a < r < 2.2a$. Physically the change in the sedimentation velocity is caused by the fact that two spheres sediment faster when they are close together than when they are far apart. Hence, a repulsive interaction, which corresponds to negative values of γ, reduces the sedimentation rate beyond the hard-sphere contribution K_1/K_0, where $K_1/K_0 < 0$. Repulsive interactions therefore increase the driving force for gradient diffusion, while simultaneously reducing the effective hydrodynamic mobility of the particles. For most conditions of interest, including those in our experiments, the net effect of a repulsive interaction is to increase the rate of diffusion relative to the hard-sphere prediction.

4. Measuring rates of diffusion by holographic interferometry

In order to measure rates of diffusion in gels we have used a technique known as holographic interferometry (Kosar & Phillips 1995; Kong *et al.* 1997). In a holographic interferometry experiment, a concentration gradient is imposed throughout a gel over macroscopic dimensions, and subsequent changes in the solute concentration are monitored via interference fringes that are generated from laser light. The fact that the diffusion is monitored over macroscopic distances helps to minimize the effects of local heterogeneities in the gel, and the presence of the concentration gradient results

in the measurement yielding a gradient diffusion coefficient, suitable for comparison with the theory developed above.

Holographic interferometry measurements were used to study diffusion of oc-taethylene glycol monododecyl ether ($C_{12}E_8$) micelles and the protein bovine serum albumin (BSA) in agarose gels. These two solutes are of comparable size: BSA has a hydrodynamic radius between 3.3 and 3.5 nm (Wattenbarger *et al.* 1992; Kong *et al.* 1997), while $C_{12}E_8$ micelles are somewhat smaller (2.7–3.1 nm) (Nilsson & Lindman 1983; Matsumoto & Zenkoh 1990; Kong *et al.* 1997). Both solutes are small enough to be Brownian, yet large enough for hydrodynamic interactions to be important. Such nanometre-scale particles are an industrially and biologically significant class of solutes. Indeed, diffusion of proteins and surfactant aggregates in gels plays an important role in membrane, chromatographic, and electrophoretic separations, in controlled release technologies and drug delivery (Park, Cohen & Langer 1992; Lawrence 1994; Saltzman *et al.* 1994; Dunmire & Katz 1997; Haller & Saltzman 1998), and in solute extraction (Hurter & Hatton 1992; Calvert, Phillips & Dungan 1994).

In the thermodynamic and hydrodynamic theories developed above, the concentration dependence of diffusion of colloidal solutes in gels is predicted for spherical solutes with a short-range interaction potential. It is therefore worth considering how appropriate it is to apply such a description to the micellar aggregates and proteins studied experimentally in this work. Micelles are often spherical aggregates of surfactants which spontaneously self-assemble in aqueous solution. As such, the size and shape of the aggregate is a function of the aqueous environment in which the aggregate forms, and the aggregate itself is in a state of dynamic equilibrium, with individual surfactant molecules continually entering and leaving. Therefore, one's ability to treat the micelle as a sphere depends on the extent to which the micelle's properties change within a gel environment. In aqueous solution and at room temperature, $C_{12}E_8$ is known to form monodisperse, spherical micelles whose properties are not strongly temperature or concentration dependent (Puvvada & Blankschtein 1990; Almgren & Alsins 1991; Carale & Blankschtein 1992; Johansson, Hedberg & Lofroth 1993; Medhage & Alsins 1993; Danino, Talmon & Zana 1997). Furthermore, measurements of diffusion (Penders *et al.* 1993; Kong *et al.* 1997) and aggregation number (Nolan, Phillips & Dungan 1999) have indicated that the size of these micelles is not affected by the presence of agarose gels. Diffusion of $C_{12}E_{18}$ micelles in agarose gels at infinitely dilute solute concentrations has been accurately predicted by modelling the micelles as spheres (Kong *et al.* 1997). These prior results provide support for our approach of representing micelles as sphere with an allowance for a short-range, solute–solute interaction.

In some respects, it is more apparent that a modified hard-sphere model is an appropriate representation of the protein BSA than a micelle. As a compact, globular protein, the size and shape of BSA is not likely to be altered significantly in the presence of the gel fibres. However, in contrast to the nonionic $C_{12}E_8$ micelles, protein molecules contain some charged amino acid groups, so that the contribution of electrostatic interactions to diffusion must be considered. In order to minimize such contributions, our holographic interferometry experiments with BSA were carried out in the presence of 0.15 M KCl; previous results at dilute solute concentrations indicate that, at such an ionic strength, BSA diffusion is at most only weakly affected by electrostatic interactions (Kosar & Phillips 1995; Johnson *et al.* 1995). Furthermore, the Debye length in an aqueous solution of 0.15 M KCl at 25 °C is approximately 0.75 nm, nearly five times smaller than the radius of BSA. Hence, to the extent that
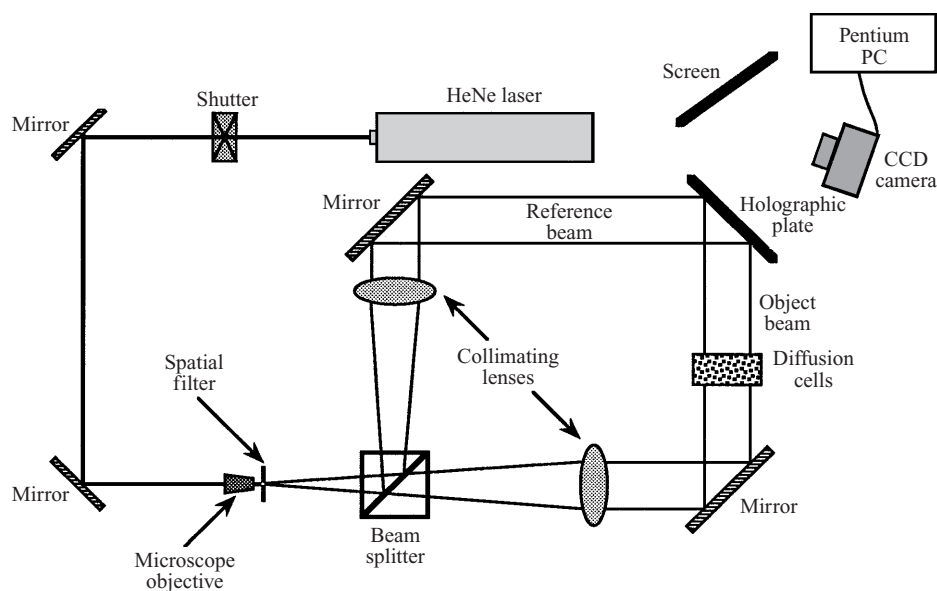
FIGURE 5. Schematic diagram of the holographic interferometer.

non-hydrodynamic interactions do take place, incorporating a short-range interaction potential into the theory should account for them.

Agarose, the gel used in our experimental studies, is formed from a nonionic polysaccharide polymer containing primarily β-D-galactopyranose and $3, 6$-anhydro-α-L-galactopyranose glycose units. It exhibits hysteresis in its gel formation properties, in that it forms a gel upon being cooled below 20–$40\,^{\circ}$C, but remains in the gel state upon reheating until the temperature rises above 60–$90\,^{\circ}$C. Electron micrographs and other experimental measurements on this gel show it to be an interconnected network of fibres in an open structure, with a mean pore diameter on the order of 25–$50\,$nm (Stellwagen 1985, 1992; Holmes & Stellwagen 1990; Stellwagen & Holmes 1990; Westrin 1991; Chui, Phillips & McCarthy 1995). Small-angle x-ray scattering (SAXS) experiments have shown that the radii of the fibres in agarose gels have a bimodal distribution, with approximately 13% of them having a mean radius of $4.5\,$nm and 87% having a mean radius of $1.5\,$nm (Djabrourov et al. 1989).

The diffusion cell for a holographic interferometry measurement is a $4\,$cm $\times$ $1\,$cm $\times$ $0.5\,$cm spectrophotometric cuvette. To begin an experiment, a solution of agarose polymer and solute is added to the cuvette until it is half-filled, and the solution is allowed to cool. The agarose used here gels at $27\,^{\circ}$C, so that proteins and other temperature-sensitive solutes can be mixed under mild conditions before gelation occurs. After this first gel has formed, a second agarose solution containing a slightly higher solute concentration is introduced at the bottom of the cuvette by using a syringe. Adding the second solution from the bottom of the cuvette causes the first gel to slide upwards, resulting in a flat interface between the two regions at a position approximately half-way between the top and bottom of the cuvette. The cooling time required for the bottom gel is approximately 5 minutes.

After the two regions of gel have been put in place and allowed to cool, the cuvette is left for 2–3 hours, during which time the step change in concentration at the gel/gel interface at $x = 0$ relaxes slightly. After this waiting period, a holographic image of the diffusion cell is made, at time t_1. As shown in figure 5, the apparatus
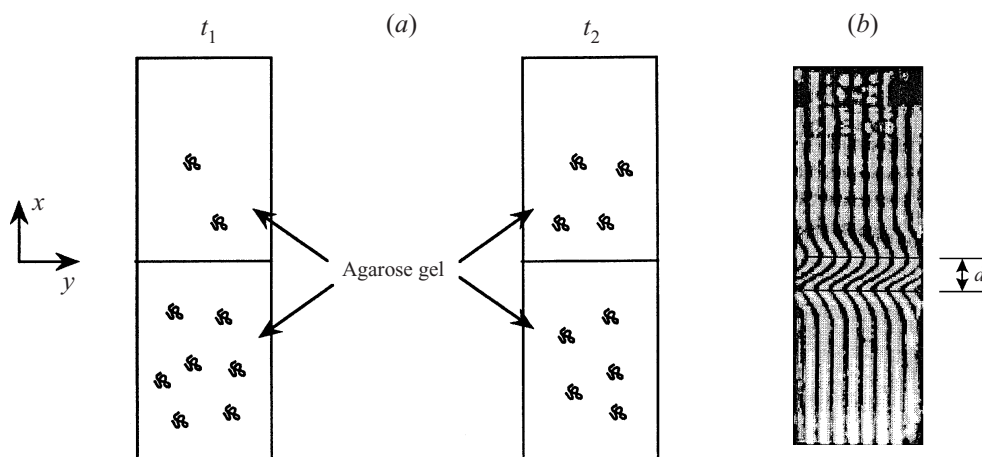
FIGURE 6. (*a*) Schematic diagram of a diffusion cell and (*b*) interference fringes from a diffusion experiment.

for making the image consists of a 10 mW HeNe laser, which produces light that is filtered and split into an 'object' beam and a 'reference' beam. The latter is needed for exposure of the holographic plate; it is not a reference beam in the sense of traditional interferometry. The object beam passes through the temperature-controlled diffusion cell, while the reference beam impinges directly on the plate. A projection of the hologram and the object beam onto a white screen exhibits the interference fringes, which are monitored continuously by a CCD camera that is connected to a Pentium personal computer.

The optical image that is stored in the holographic plate at time t_1 provides a reference for monitoring solute diffusion in the vertical direction. This image is superimposed on the actual cell at a later time t_2, when the diffusion process has caused changes in concentration which in turn cause changes in the refractive index. At vertical positions where the optical path length of the light changes by odd multiples of one-half of the wavelength, destructive interference occurs and horizontal interference fringes form. In our experiments, we find it convenient to tilt slightly the mirror that directs the object beam through the diffusion cell. This change is made after exposure of the holographic plate, but before the fringes are analysed, and it has the effect of introducing a linear y-dependence into the change in optical path length (cf. figure 6). If the mirror is tilted by a small angle α, then the dark fringes form at positions where

$$m\Delta c(z, t_1, t_2) - \alpha y = (2j - 1)\pi/k_\lambda \quad \text{for} \quad j = 1, 2, 3\ldots. \tag{76}$$

In (76), Δc is the concentration change, and m is a constant as long as refractive index and concentration are linearly related. The wavenumber k_λ in (76) is given by $k_\lambda = 2\pi/\lambda$, where λ is the wavelength of the light, or 632.8 nm for the HeNe laser.

An actual interference pattern obtained after tilting the object beam is shown in figure 6(*b*), and consists of a pattern of vertical fringes that bend to form maxima and minima in the region near the gel/gel interface. This form can be calculated theoretically by using the solution for the concentration change Δc

$$\Delta c = \frac{1}{2}\left[\operatorname{erf}\left(\frac{x}{\sqrt{4Dt_1}}\right) - \operatorname{erf}\left(\frac{x}{\sqrt{4Dt_2}}\right)\right]\Delta c_0, \tag{77}$$

where Δc_0 is the initial concentration difference. Equation (77) is valid for times t such that $t \ll L^2/D$, so that the influences of the top and the bottom of the gel can be neglected. In addition, this result is derived under the assumption that the effect of concentration variations on diffusion are negligible, so that D is constant. Substituting (77) into (76) and differentiating shows that the separation d between the extrema is related to the diffusion coefficient D by

$$D = \frac{d^2}{8} \frac{(1/t_1 - 1/t_2)}{\ln(t_2/t_1)}. \tag{78}$$

From a single experiment, several values of D can be obtained by measuring a series of separations d at successively longer times t_2.

The agarose and BSA used for the experiments were purchased from Sigma Chemical Co. As mentioned above, the Type VII agarose that was used transitions from a liquid to a gel at $27\,^\circ\text{C}$, allowing BSA to be mixed and stirred thoroughly at temperatures that do not lead to denaturation. The $C_{12}E_8$ surfactant was purchased from Fluka, and the KCl was purchased from Fisher Scientific. All reagents were used as supplied, and all solutions and gels were prepared with distilled, deionized water ($10\text{–}18\,\text{m}\Omega$).

The components of the holographic interferometer are described by Kosar & Phillips (1995) and Kong *et al.* (1997), although minor modifications have been made to the apparatus since that work was completed. For the gel experiments, a device was constructed that holds two cuvettes so that two samples can be studied simultaneously. The device is made of copper, which surrounds both cuvettes on four sides, the front and back being left open to allow the object beam to pass through the gel. Water circulated through tubing at the base of this cuvette-holder is used to control the temperature at $25 \pm 0.8\,^\circ\text{C}$, as monitored by a probe that is located in a copper sleeve between the two cuvettes. For liquid samples, use of the temperature controller caused convection currents that disturbed the liquid/liquid interface and fringes. Liquid experiments were therefore conducted at room temperature, which was $22 \pm 1.5\,^\circ\text{C}$, and the results were adjusted to $25\,^\circ\text{C}$ by using the fact that the ratio $D\mu/T$ is a constant.

5. Results and discussion

5.1. *Numerical results*

The theories developed above can be used to determine the dependence of diffusion on solute concentration. For hard spheres this dependence is quantified by the coefficient

$$\frac{D_1}{D_0} = 1 + \frac{7}{\kappa_0} + \frac{K_1}{K_0}, \tag{79}$$

which appears in the expansion $D/D_0 = 1 + \phi D_1/D_0$, in which the normalization coefficient D_0 describes the rate of diffusion in the gel at infinitely dilute solute concentrations. The concentration here is based on total volume of the gel, including both fluid and fibres. The coefficient D_1/D_0 contains thermodynamic contributions through the parameter κ_0, and hydrodynamic contributions through K_1 and K_0. Equation (79) allows one to predict the strength of the concentration dependence in the gel relative to that in aqueous solution, and to evaluate the relative importance of thermodynamic and hydrodynamic contributions to that dependence.

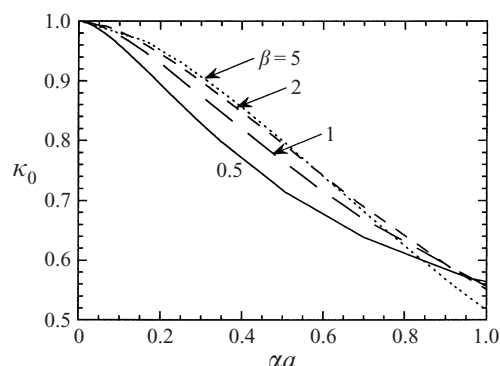Equation (12) indicates that the parameter κ_0 depends on the fibre volume fraction

FIGURE 7. Plot of the infinite-dilution partition coefficient κ_0 as a function of αa for ratios of the solute-to-fibre radius $\beta = 0.5$, 1, 2 and 5.

ϕ_f and the ratio $\beta = a/a_f$ of the solute radius to the fibre radius. The hydrodynamic coefficients K_1 and K_0 are functions only of αa, the ratio of solute size to the square root of the hydraulic permeability k. However, using the relation for k developed by Jackson & James (1986).

$$\frac{k}{a_f^2} = \frac{-3}{20} \frac{(\ln \phi_f + 0.931)}{\phi_f}, \tag{80}$$

one finds that αa can be expressed as $\beta/f(\phi_f)$, where $f(\phi_f)$ is a function of fibre volume fraction only. Using this relation and the development in §§ 2 and 3, the contributions of κ_0 and K_1/K_0 to D_1/D_0 can be calculated as functions of only β and ϕ_f. In these calculations we consider only cases where the gel is sufficiently dilute so that the solute has access to most of the pore space, as determined by the requirement that $\kappa_0 > 0.75$. It is under these conditions that near-field hydrodynamic solute–fibre interactions are likely to be relatively less important, so that the approximations made in the theoretical development above are most appropriate. In figure 7 the partition coefficient κ_0 is shown as a function of αa for several values of the ratio β. Inspection of these curves indicates that restriction to values of $\alpha a \leqslant 0.4$ allows the above constraint on the partitioning behaviour to be met.

In figure 8(*a–c*), curves for $7/\kappa_0, -K_1/K_0$ and D_1/D_0 are shown as a function of fibre volume fraction for values of β equal to 0.5, 1 and 5. Clearly D_1/D_0 is significantly augmented in the gel for all values of β, i.e. the theory predicts a stronger concentration dependence of solute diffusion in the gel than in aqueous solution. Over the range of fibre volume fraction and size ratios considered here, D_1/D_0 is increased more than four-fold: from $D_1/D_0 = 1.45$ in aqueous solution to $D_1/D_0 = 5$– 6 in the gel. The influence of the gel on this concentration dependence increases with increasing fibre volume fraction. This effect is a result of changes in both the thermodynamics and hydrodynamics inside the gel: increasing fibre volume fraction decreases the zero-order partition coefficient κ_0, and also decreases the magnitude of the hydrodynamic coefficient K_1/K_0. Since the latter is a negative contribution to D_1/D_0, the solute concentration effect is a result of an increase of the thermodynamic effect ($7/\kappa_0$ increases as ϕ_f increases) combined with a decrease in the strength of the solute–solute hydrodynamic interactions inside the fibrous medium. Both of these changes are comparable, and therefore the enhancement in D_1/D_0 cannot be attributed to either effect alone.

Since the results in figure 8 were calculated over the same range of αa in all three
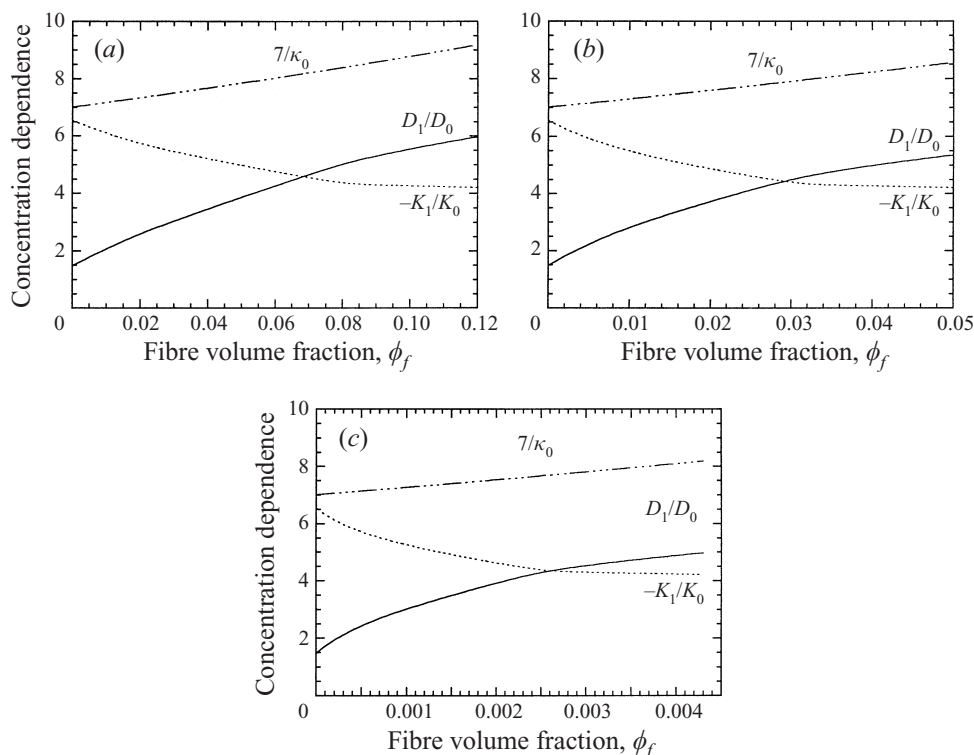
FIGURE 8. Thermodynamic and hydrodynamic contributions to the concentration dependence are plotted vs. the fibre volume fraction ϕ_f for ratios of the solute-to-fibre radius of (a) $\beta = 0.5$, (b) $\beta = 1.0$ and (c) $\beta = 5.0$.

cases, it is apparent that the magnitude of the changes in $7/\kappa_0$, K_1/K_0 and D_1/D_0 differs only slightly for the three values of β. However, what does change substantially as β is varied is the range of fibre volume fractions over which the enhancement in D_1/D_0 is observed. For the case where the solute is half as large as the fibre, $\beta = 0.5$, the fibre volume fraction must be as high as 10% for D_1/D_0 to exceed 5.0. At such a low value of β, fewer fibres are needed to achieve a given volume fraction, and the result in a relatively porous gel in which the influence of fibres on solute partitioning or viscous interaction is weak. In contrast, as β increases one observes a decrease in the gel concentration needed to effect a given enhancement in D_1/D_0. At $\beta = 1$ only a 5% gel is needed to reach $D_1/D_0 = 5$, whereas at $\beta = 5$ the same effect is present at $\phi_f = 0.5\%$. Thus, in the case where the gel fibres are thin relative to the solute, diffusion is strongly affected because so many more fibres are present at a given ϕ_f.

5.2. *Comparison with experimental data*

Measured diffusion coefficients of $C_{12}E_8$ micelles in aqueous solution are plotted as a function of solute volume fraction in figure 9. These experiments, and those described below, were performed with an initial concentration difference Δc_0 of 1 wt % surfactant. The conversion from weight percent to volume fraction is made by using an aggregation number of 79.4 (Johansson *et al.* 1993) and a surfactant molecular weight of 538.77, and the volume fractions reported are an average of those in the lower (i.e. surfactant-rich) and upper (i.e. surfactant-poor) regions of the cuvette. Extrapolation of the data to obtain the infinite-dilution diffusivity D_0 yields
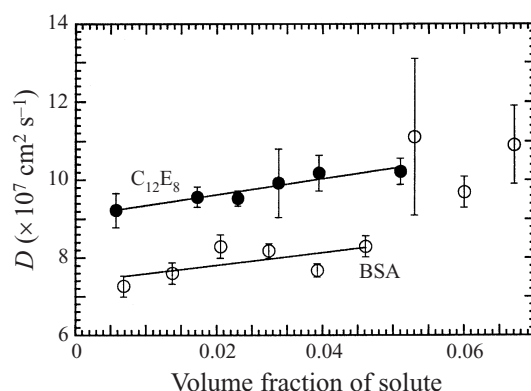
FIGURE 9. Diffusion coefficients for $C_{12}E_8$ and BSA solutes in aqueous solution are plotted as a function of solute volume fraction.
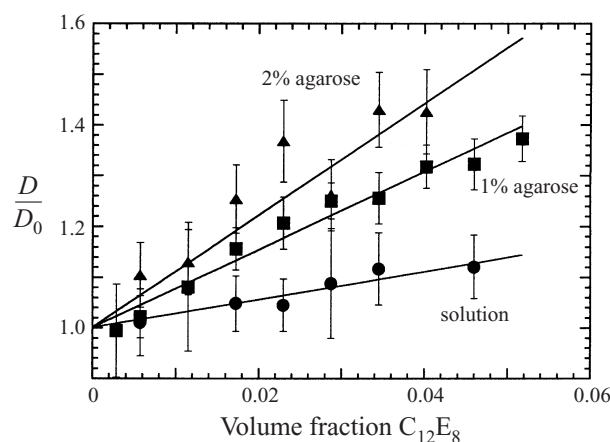

FIGURE 10. Normalized diffusion coefficients of $C_{12}E_8$ in aqueous solution, in 1 wt % agarose gel, and in 2 wt % agarose gel are plotted as a function of solute volume fraction.

a value of $9.12 \pm 0.41 \times 10^{-7}$ cm^2 s^{-1} at 25 °C, which corresponds to a Stokes–Einstein radius of 2.7 ± 0.12 nm. This hydrodynamic radius is in good agreement with results reported previously (Nilsson & Lindman 1983; Matsumoto & Zenkoh 1990; Kong *et al.* 1997).

To evaluate the effect of solute concentration, one can normalize the data by D_0 and evaluate the slope of a line fit to a plot of D/D_0 vs. ϕ. For the data shown in figure 9, the resulting line has a slope of 2.8 ± 1.4, in reasonable agreement with, but somewhat higher than, the value of 1.45 predicted by Batchelor (1976). The uncertainties in the slopes reported here represent 95% confidence limits on the slope of a plot of D vs. ϕ, modified to account for the uncertainty in the normalization coefficient D_0. Results for the protein BSA, measured at a KCl concentration of 0.15 M and a pH of 6.9, are also shown in figure 9. For those data, the measured Stokes–Einstein radius was 3.3 ± 0.13 nm, and the slope of the line obtained by plotting D/D_0 vs. ϕ was 3.0 ± 1.6. Unlike the nonionic micelles, the plot for the BSA became nonlinear at the higher volume fractions, and hence the slope was calculated using data in the range $0 < \phi < 4\%$.

In figure 10, diffusion coefficients for the $C_{12}E_8$ micelles are plotted as a function
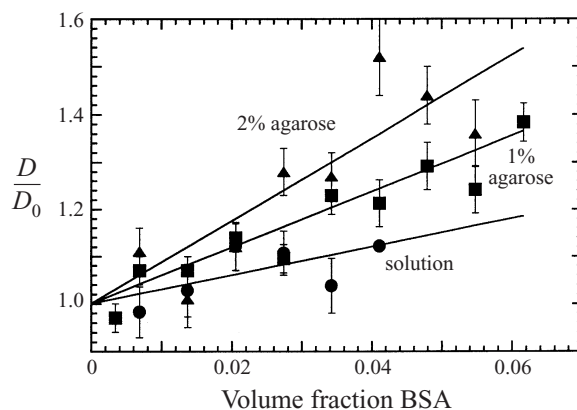
FIGURE 11. Normalized diffusion coefficients for BSA in aqueous solution, in 1 wt % agarose gel, and in 2 wt % agarose gel are plotted as a function of solute volume fraction.

of micelle volume fraction in solution and in agarose gels. Gel concentrations of 1 wt % and 2 wt % are considered, and the diffusion data are normalized by D_0, the diffusion coefficient extrapolated to zero solute volume fraction at a particular gel concentration. For all three cases the data show the expected trend, with the normalized diffusion coefficient increasing linearly with concentration. Furthermore, the slopes of the lines increase with increasing concentration, being 2.8 ± 1.4 in pure solution, 7.7 ± 1.3 in the 1 wt % gel, and 11.0 ± 2.5 in the 2 wt % gel. This trend of a stronger concentration dependence in the gel is consistent with predictions of the theory described above.

By using (80) above in conjunction with (20) in Clague & Phillips (1997) to account for the bimodal nature of the fibre radii, we estimate the hydraulic permeability of the agarose to be such that $\alpha = 0.085\,\mathrm{n\,m^{-1}}$ for the 1 wt % gel and $\alpha = 0.132\,\mathrm{n\,m^{-1}}$ for the 2 wt % gel, yielding αa values of 0.23 and 0.36, respectively, for the micelles. For these parameter values, the methods of §3 (cf. (79)) predict slopes of 3.7 and 5.1 for the 1 and 2 wt % gels, respectively. Hence, the theory is in qualitative agreement with the data, although it underpredicts the size of the concentration effect. We note, however, that the approximation inherent in modelling the solutes as hard spheres and the gel as a random fibre matrix, which is further simplified to a Brinkman medium, introduces uncertainty in the theoretical predictions, and the agreement between theory and experiment may thus be considered reasonable. The agreement is improved considerably by incorporating a short-range repulsion into the theoretical prediction, as discussed below.

Diffusion coefficients for BSA, again normalized by the appropriate infinite-dilution value, are plotted in figure 11. In this case, solute concentrations were converted to volume fractions by using the measured 3.3 nm radius of the BSA and a molecular weight of 67 000. As with the $C_{12}E_8$, results are shown for pure solution, 1 wt % and 2 wt % agarose gel. The results are quantitatively similar to those shown in figure 10. Each set of data shows a linear increase in D/D_0 with solute concentration, and the slopes increase from 3.0 ± 1.6 for the pure solution to 5.9 ± 0.9 and 8.7 ± 1.5 in the 1 and 2 wt % gels, respectively. These measured slopes are to be compared with the predicted values of 4.2 and 5.7, showing that the theory again underpredicts the strength of the effect, although less so for BSA than for $C_{12}E_8$ micelles.

The hydrodynamic and thermodynamic theories presented above are based upon

System	αa	κ_0	D_1/D_0 Theory ($\gamma = 0$)	D_1/D_0 Theory ($\gamma \neq 0$)	D_1/D_0 Experiment
$C_{12}E_8$				($\gamma = -4.5$)	
Solution	0	1.0	1.45	4.0	2.8 ± 1.4
1% agarose	0.23	0.93	3.7	7.1	7.7 ± 1.3
2% agarose	0.36	0.87	5.1	9.2	11.0 ± 2.5
BSA				($\gamma = -2.1$)	
Solution	0	1.0	1.45	2.6	3.0 ± 1.6
1% agarose	0.28	0.91	4.2	5.9	5.9 ± 0.9
2% agarose	0.43	0.83	5.7	7.8	8.7 ± 1.5

TABLE 2. Effect of concentration on hindered diffusion: comparison of theory and experiment.

a representation of agarose as a homogeneous medium of straight, cylindrical fibres. It is worth noting, however, that there is some evidence of inhomogeneities in these gels. Johnson & Deen (1996) have measured the permeability of agarose by imposing a pressure-driven flow through 70–100 µm thick agarose membranes. At high concentrations, $\phi_f > 0.05$, their data are in reasonable agreement with (80), but at low concentrations their measured permeabilities were four to seven times larger than the predicted values. Since (80) agrees quantitatively with numerical calculations of permeabilities in homogeneous, three-dimensional arrays of fibres (Higdon & Ford 1996; Clague & Phillips 1997), these deviations are presumably caused by inhomogeneities in the gel.

Increasing the permeability by a factor of four in our calculations corresponds to using $\alpha = 0.043$ nm^{-1} for the 1 wt% gel and 0.066 nm^{-1} for the 2 wt% gel. Under these conditions, the predicted slopes of the lines formed by plotting D/D_0 vs. ϕ are lowered to 2.9 and 3.9 for the micelles and 3.2 and 4.6 for the BSA in the 1 and 2 wt% gels, respectively. Hence, the qualitative behaviour is unchanged, but the theory underpredicts the data to a greater extent than it does with the permeabilities calculated from (80). One would expect the hydraulic permeability to be more sensitive to inhomogeneities or microchannels in the gel than the diffusion coefficient. Hence, it would appear that attempting to account for the effects of structural inhomogeneities on diffusion by inserting a corrected permeability into the theory may cause the effect of the gel fibres to be underestimated. In the discussion below we refer to values of αa calculated from (80) in conjunction with (20) in Clague & Phillips (1997).

The experimentally measured slopes of the lines in figures 10 and 11 are summarized in table 2. Also shown are the theoretically predicted slopes, both with ($\gamma \neq 0$) and without ($\gamma = 0$) an additional repulsive interaction potential. Without an interaction potential, the measured effect of concentration on D/D_0 is consistently greater than what is predicted for hard-sphere solutes. However, choosing $\gamma = -4.5$ for the $C_{12}E_8$ micelles yields slopes that are within the confidence intervals shown both for diffusion in pure solution and in the 1% and 2% agarose gels. Since $C_{12}E_8$ micelles have no electrostatic charge, the solute–solute repulsion is presumably caused by steric interaction between the hydrophilic head groups of the micelles. Such steric repulsion is partly accounted for in our treatment of the micelles as hard spheres with a size given by the hydrodynamic radius, but an additional 'soft-sphere' repulsion may be needed to fully account for the influence of surfactant headgroup overlap forces.

One can estimate the strength of these forces by using scaling arguments originally developed by de Gennes for the overlap of polymer brushes (de Gennes 1987; Israelachvili & Wennerstrom 1992). The resulting expression for the steric repulsive energy Φ/kT between two spheres with radius a is (McClements & Dungan 1997)

$$\frac{\Phi}{kT} = 64\pi\frac{aL^2}{s^3}\left[\frac{1}{5}\left(\frac{2L}{\Delta}\right)^{1/4} + \frac{3}{35}\left(\frac{\Delta}{2L}\right) - \frac{1}{77}\left(\frac{\Delta}{2L}\right)^{11/4} - \frac{3}{11}\right] \quad \text{for} \quad \Delta < 2L, \quad (81)$$

where L is the thickness of the chain region, s is the lateral distance between chains, and Δ is the surface to surface separation. The distance s may be estimated by dividing the surface area of the hard-sphere region by the micelle aggregation number. By substituting (81) into (73) and using $\gamma = -4.5$, one finds that a thickness $L = 6\,\text{Å}$ corresponds to the region of 'soft-sphere' overlap repulsion. This value of L appears to be quite reasonable, considering the molecular structure of $C_{12}E_8$ micelles. Molecular theories for the self-assembly of these surfactants (Naor, Puvvada & Blankschtein 1992; Carale, Pham & Blankschtein 1994) indicate that the radial distance from the micelle centre to the edge of the headgroup region is approximately $35\,\text{Å}$. Thus, the surfactant headgroups project approximately $8\,\text{Å}$ beyond the hydrodynamic radius of $27\,\text{Å}$ used in our model of $C_{12}E_8$, close to the value of $6\,\text{Å}$ estimated from (73) and (81).

A smaller short-range interaction, for which $\gamma = -2.1$, similarly increases the predicted slopes for BSA such that all three values lie within the indicated 95% confidence intervals for the data. As noted above, at an ionic strength of $0.15\,\text{M}$ the Debye length in an aqueous solution of KCl is approximately $0.75\,\text{nm}$. This value may be substituted into the Derjaguin expression for the interaction of two charged spheres

$$\frac{\Phi}{kT} = 2\pi\frac{\varepsilon a\phi_0^2}{kT}\ln\left(1 + e^{-\kappa\Delta}\right), \quad (82)$$

allowing an estimate to be obtained for the value of γ arising from electrostatic interactions. In (82) ε is the aqueous dielectric permittivity, and ϕ_0 is the surface potential of the BSA. Substitution of this expression into (73) indicates that the value of $\gamma = -2.1$ shown in table 2 corresponds to a surface potential of $\phi_0 = -13\,\text{mV}$. This value is comparable in size to experimentally measured values ($\phi_0 \approx -20\,\text{mV}$) for BSA in solutions with an ionic strength of $0.15\,\text{M}$ and a pH near 7.0 (Vilker, Colton & Smith 1981; Bowen & Williams 1996).

For both nonionic and ionic solutes, it is assumed above that the interaction energy Φ is short-range relative to the size of the particle. For both types of colloidal particles this assumption of a short-range potential is reasonable. Although the criterion that $\exp\left(-\Phi/kT\right) - 1 \approx 0$ for $r > 2.2a$ is not strictly satisfied in either case, it is true that $\exp\left(-\Phi/kT\right) - 1 \approx 0$ for $r > 2.5a$, and the error resulting from the approximation used for the mobility functions in the expression (74) does not affect the comparison significantly given the experimental uncertainty in the measured slopes. Overall we therefore conclude that, for both nonionic micelles and charged protein solutes, the values given in table 2 realistically capture the size of short-range interactions between the particles. In the case of $C_{12}E_8$ micelles, these interactions arise primarily from overlap forces not captured in the hard-sphere interactions, and in the case of BSA electrostatic forces are responsible for this effect. Note that in the above independent estimates for these interactions the influence of attractive Van der Waals forces is neglected. Including them would counteract in part the repulsive steric and

electrostatic interactions mentioned, improving the agreement between the estimated and measured interaction parameter γ.

6. Conclusion

The effects of solute concentration on hindered gradient diffusion in rigid, fibrous porous media can be separated into two primary mechanisms. First, the volume excluded by the fibres increases the strength of the thermodynamic interactions between solutes by increasing the effective solute concentration in the liquid phase. In addition, hydrodynamic interactions between the solutes are screened by the immobile fibres, which act as an effective or Brinkman porous medium. For gels in which steric or excluded-volume interactions are dominant, and energetic interactions are significant only over short distances, these influences tend to increase the effect of concentration on hindered gradient diffusion relative to gradient diffusion in pure solution. It has been shown here that mathematical predictions derived from these physical concepts are in good agreement with experimental data, providing evidence that both thermodynamic and hydrodynamic interactions play important roles in hindered diffusion in microporous gels.

REFERENCES

ALMGREN, M. & ALSINS, J. 1991 Fluorescence quenching in 3-dimensions to zero-dimension – effect of dimensionality on a diffusion-limited reaction. *Is. J. Chem.* **31**, 159.

BATCHELOR, G. K. 1972 Sedimentation in a dilute dispersion of spheres. *J. Fluid Mech.* **52**, 245.

BATCHELOR, G. K. 1976 Brownian diffusion of particles with hydrodynamic interaction. *J. Fluid Mech.* **74**, 1.

BATCHELOR, G. K. 1982 Sedimentation in a dilute polydisperse system of interacting spheres. Part 1. General theory. *J. Fluid Mech.* **119**, 379.

BATCHELOR, G. K. 1983 Diffusion in a dilute polydisperse system of interacting spheres. *J. Fluid Mech.* **131**, 155.

BATCHELOR, G. K. & WEN, C.-S. 1982 Sedimentation in a dilute polydisperse system of interacting spheres. Part 2. Numerical results. *J. Fluid Mech.* **124**, 495.

BOWEN, W. R. & WILLIAMS, P. M. 1996 Dynamic ultrafiltration model for proteins: A colloidal interaction approach. *Biotech. Bioengng* **50**, 125.

BRENNER, H. 1964 The Stokes resistance of an arbitrary particle–IV. Arbitrary fields of flow. *Chem. Engng Sci.* **19**, 703.

BRINKMAN, H. C. 1947 A calculation of the viscous force exerted by a flowing fluid on a dense swarm of particles. *Appl. Sci. Res.* A **1**, 27.

CALVERT, T. L., PHILLIPS, R. J. & DUNGAN, S. R. 1994 Extraction of naphthalene by block copolymer surfactants immobilized polymeric hydrogels. *AIChE J.* **40**, 1449.

CARALE, T. R. & BLANKSCHTEIN, D. 1992 Theoretical and experimental determinations of the crossover from dilute to semidilute regimes of micellar solutions. *J. Phys. Chem.* **96**, 459.

CARALE, T. R., PHAM, Q. T. & BLANKSCHTEIN, D. 1994 Salt effects on intramicellar interactions and micellization of nonionic surfactants in aqueous solutions. *Langmuir* **10**, 109.

CHUI, M. M., PHILLIPS, R. J. & MCCARTHY, M. J. 1995 Measurement of the porous microstructure of hydrogels by nuclear magnetic resonance. *J. Colloid Interface Sci.* **174**, 336.

CLAGUE, D. S. & PHILLIPS, R. J. 1996 Hindered diffusion of spherical macromolecules through dilute fibrous media. *Phys. Fluids* **8**, 1720.

CLAGUE, D. S. & PHILLIPS, R. J. 1997 A numerical calculation of the hydraulic permeability of three-dimensional disordered fibrous media. *Phys. Fluids* **9**, 1562.

DABROS, T. 1985 A singularity method for calculating hydrodynamic forces and particle velocities in low-Reynolds-number flows. *J. Fluid Mech.* **156**, 1.

DANINO, D., TALMON, Y. & ZANA, R. 1997 Aggregation and microstructure in aqueous solutions of the nonionic surfactant C(12)E(8). *J. Colloid Interface Sci.* **186**, 170.

DEEN, W. M. 1987 Hindered transport of large molecules in liquid-filled pores. *AIChE J.* **33**, 1409.

DEEN, W. M. 1998 *Analysis of Transport Phenomena.* Oxford University Press.

DJABROUROV, M., CLARK, A. H., ROWLANDS, D. W. & ROSS-MURPHY, S. B. 1989 Small-angle X-ray scattering characterization of agarose sols and gels. *Macromolecules* **22**, 180.

DUNMIRE, E. N. & KATZ, D. F. 1997 Measurement and modulation of nonoxynol-9 diffusion and bioactivity against spermatozoa in human cervical mucus. *Contraception* **55**, 115.

DURLOFSKY, L. & BRADY, J. F. 1987 Analysis of the Brinkman equation as a model for flow in porous media. *Phys. Fluids* **30**, 3329.

DURLOFSKY, L., BRADY, J. F. & BOSSIS, G. 1987 Dynamic simulation of hydrodynamically interacting particles. *J. Fluid Mech.* **180**, 21.

FANTI, L. R. & GLANDT, E. D. 1990 Partitioning of spherical particles into fibrous matrices. 1. Density-functional theory. *J. Colloid Interface Sci.* **135**, 385.

GENNES, P. G. DE 1987 Polymers at an interface; a simplified view. *Adv. Colloid Interface Sci.* **27**, 189.

GOLDMAN, A. J., COX, R. G. & BRENNER, H. 1966 The slow motion of two identical arbitrarily oriented spheres through a viscous fluid. *Chem. Engng Sci.* **21**, 1151.

GUSTAFSSON, N. O., WESTRIN, B., AXELSSON, A. & ZACCHI, G. 1993 Measurement of diffusion coefficients in gels using holographic laser interferometry. *Biotechnol. Prog.* **9**, 436.

HALLER, M. F. & SALTZMAN, W. M. 1998 Localized delivery of proteins in the brain: Can transport be customized? *Pharm. Res.* **15**, 377.

HIGDON, J. J. L. & FORD, G. D. 1996 Permeability of three-dimensional models of fibrous porous media. *J. Fluid Mech.* **308**, 341.

HINCH, E. J. 1977 An averaged-equation approach to particle interactions in a fluid suspension. *J. Fluid Mech.* **83**, 695.

HOLMES, D. L. & STELLWAGEN, N. C. 1990 The electric field dependence of DNA mobilities in agarose gels – A reinvestigation. *Electrophoresis* **11**, 5.

HOWELLS, I. D. 1974 Drag due to the motion of a Newtonian fluid through a sparse random array of small fixed rigid objects. *J. Fluid Mech.* **64**, 449.

HURTER, P. N. & HATTON, T. A. 1992 Solubilization of polycyclic aromatic hydrocarbons by poly (ethylene oxide-propylene oxide) block copolymer micelles – Effects of polymer structure. *Langmuir* **8**, 1291.

ISRAELACHVILI, J. N. & WENNERSTROM, H. 1992 Entropic forces between amphiphilic surfaces in liquids. *J. Phys. Chem.* **96**, 520.

JACKSON, G. W. & JAMES, D. F. 1986 The permeability of fibrous porous media. *Can. J. Chem. Engng* **64**, 364.

JOHANSSON, L., HEDBERG, P. & LOFROTH, J. 1993 Diffusion and interaction in gels and solutions: 5. Nonionic micellar systems. *J. Phys. Chem.* **97**, 747.

JOHNSON, E. M., BERK, D. A., JAIN, R. K. & DEEN, W. M. 1995 Diffusion and partitioning of proteins in charged agarose gels. *Biophys. J.* **68**, 1561.

JOHNSON, E. M., BERK, D. A., JAIN, R. K. & DEEN, W. M. 1996 Hindered diffusion in agarose gels: Test of effective medium model. *Biophys. J.* **70**, 1017.

JOHNSON, E. M. & DEEN, W. M. 1996 Hydraulic permeability of agarose gels. *AIChE J.* **42**, 1220.

KIM, S. & RUSSEL, W. B. 1985a Modelling of porous media by renormalization of the Stokes equations. *J. Fluid Mech.* **154**, 269.

KIM, S. & RUSSEL, W. B. 1985b The hydrodynamic interactions between two spheres in a Brinkman medium. *J. Fluid Mech.* **154**, 253.

KONG, D. D., KOSAR, T. F., DUNGAN, S. R. & PHILLIPS, R. J. 1997 Diffusion of proteins and nonionic micelles in agarose gels by holographic interferometry. *AIChE J.* **43**, 25.

KOSAR, T. F. & PHILLIPS, R. J. 1995 Measurement of protein diffusion in dextran solutions by holographic interferometry. *AIChE J.* **41**, 701.

LAWRENCE, M. J. 1994 Surfactant systems – Their use in drug delivery. *Chem. Soc. Rev.* **23**, 417.

MATSUMOTO, T. & ZENKOH, J. 1990 Micelle structure in isotropic aqueous colloids of a poly (oxyethylene) amphiphile $C_{12}E_8$. *Colloid Polymer Sci.* **268**, 536.

McCLEMENTS, D. J. & DUNGAN, S. R. 1997 Effect of colloidal interactions on the rate of interdroplet heterogeneous nucleation in oil-in-water emulsions. *J. Colloid Interface Sci.* **186**, 17.

MEDHAGE, B., ALMGREN, M. & ALSINS, J. 1993 Phase structure of poly (oxyethylene) surfactants in water studied by fluorescence quenching. *J. Phys. Chem.* **97**, 7753.

NAOR, A., PUVVADA, S. & BLANKSCHTEIN, D. 1992 An analytical expression for the free energy of micellization. *J. Phys. Chem.* **96**, 7830.

NILSSON, P. G. & LINDMAN, B. 1983 Water self-diffusion in nonionic surfactant solutions: Hydration and obstruction effects. *J. Phys. Chem.* **87**, 4756.

NITSCHE, L. C. & BRENNER, H. 1990 Hydrodynamics of particle motion in sinusoidal pores via a singularity method. *AIChE J.* **36**, 1403.

NOLAN, S. L., PHILLIPS, R. J. & DUNGAN, S. R. 1999 Frequency domain fluorescence measurements of the aggregation properties of C_nE_m surfactants in agarose gels. *Langmuir* (submitted).

OGSTON, A. G. 1958 The spaces in a uniform random suspension of fibers. *Trans. Farad. Soc.* **54**, 1754.

PARK, T. G., COHEN, S. & LANGER, R. 1992 Poly (L-lactic acid)/Pluronic blends: Characterization of phase separation behavior, degradation, and morphology and use as protein-releasing matrices. *Macromolecules* **25**, 116.

PENDERS, M. H. G. M., NILSSON, S., PICULELL, L. & LINDMAN, B. 1993 Clouding and diffusion of nonionic surfactants in agarose gels and solutions. *J. Phys. Chem.* **97**, 11332.

PHILLIPS, R. J. 1995 Calculation of multisphere linearized Poisson–Boltzmann interactions near cylindrical fibers and planar surfaces. *J. Colloid Interface Sci.* **175**, 386.

PHILLIPS, R. J., DEEN, W. M. & BRADY, J. F. 1989 Hindered transport of spherical macromolecules in fibrous membranes and gels. *AIChE J.* **35**, 1761.

PHILLIPS, R. J., DEEN, W. M. & BRADY, J. F. 1990 Hindered transport in fibrous membranes and gels: Effect of solute size and fiber configuration. *J. Colloid Interface Sci.* **139**, 363.

PUVVADA, S. & BLANKSCHTEIN, D. 1990 Molecular-thermodynamic approach to predict micellization, phase behavior and phase separation of micellar solutions. 1 Application to nonionic surfactants. *J. Chem. Phys.* **92**, 3710.

SALTZMAN, W. M., RADOMSKY, M. L., WHALEY, K. J. & CONE, R. A. 1994 Antibody diffusion in human cervical mucus. *Biophys. J.* **66**, 508.

SOLOMENTSEV, Y. E. & ANDERSON, J. L. 1996 Rotation of a sphere in Brinkman fluids. *Phys. Fluids* **8**, 1119.

STELLWAGEN, N. C. 1985 Effect of the electric field on the apparent mobility of large DNA fragments in agarose gels. *Biopolymers* **24**, 2243.

STELLWAGEN, N. C. 1992 Agarose gel pore radii are not dependent on the casting buffer. *Electrophoresis* **13**, 601.

STELLWAGEN, N. C. & HOLMES, D. L. 1990 Resolution of a paradox in the electrophoresis of DNA in agarose gels. *Electrophoresis* **11**, 649.

VILKER, V. L., COLTON, C. K. & SMITH, K. A. 1981 The osmotic pressure of concentrated protein solutions: Effect of concentration and pH in saline solutions of bovine serum albumin. *J. Colloid Interface Sci.* **79**, 548.

WATTENBARGER, M. R., BLOOMFIELD, V. A., BU, Z. & RUSSON, P. S. 1992 Tracer diffusion of proteins in DNA solutions. *Macromolecules* **25**, 5263.

WESTRIN, B. A. 1991 Diffusion measurements in gels, a methodological study. PhD thesis, Lund University.